DEPARTMENT OF GEOSCIENCES AND GEOGRAPHY A81

From partial melting to lava emplacement: the petrogenesis of some Icelandic basalts

PAAVO NIKKOLA

UNIVERSITY OF HELSINKI
FACULTY OF SCIENCE

UNIVERSITY OF ICELAND

From partial melting to lava emplacement: the petrogenesis of some Icelandic basalts

PAAVO NIKKOLA

ACADEMIC DISSERTATION
To be presented, with the permission of the Faculty of Science of the University of Helsinki and the Faculty of Earth Sciences of the University of Iceland, for public examination in auditorium E204, Physicum, Kumpula, on 20th of March 2020, at 12 noon.

This doctoral dissertation is a co-operation between the University of Helsinki and the University of Iceland and will lead to a dual degree from these universities.

DEPARTMENT OF GEOSCIENCES AND GEOGRAPHY A81/ HELSINKI 2020

Cover photo: Paavo Nikkola
Back cover photo: Elísabet Pálmadóttir

Faculty of Science, University of Helsinki
Faculty of Earth Sciences, University of Iceland

Author´s address: Paavo Nikkola
Department of Geosciences and Geography
P.O.Box 64
00014 University of Helsinki
Finland
paavo.nikkola@helsinki.fi

Supervised by: Professor O. Tapani Rämö
Department of Geosciences and Geography
University of Helsinki

Professor Thorvaldur Thordarsson
Faculty of Earth Sciences
University of Iceland

Reviewed by: Professor Christian Tegner
Department of Geoscience
Aarhus University

Professor emeritus Eero Hanski
Oulu Mining School
University of Oulu

Opponent: Professor Reidar G. Trønnes
Natural History Museum, Centre for Earth Evolution and Dynamics
University of Oslo

ISSN 1798-7911
ISBN 978-951-51-4930-5 (paperback)
ISBN 978-951-51-4931-2 (PDF)
http://ethesis.helsinki.fi
Painosalama/Turku 2020

Nikkola P., 2020. *From partial melting to lava emplacement: the petrogenesis of some Icelandic basalts.* Painosalama, Turku, 47 pages, 6 figures.

Abstract

This thesis provides insights into the petrogenesis of Iceland basalts via three subprojects. The first uses olivine macrocrysts as a proxy for mantle melting conditions below Iceland, the second utilizes petrological thermobarometry to resolve the crustal storage conditions of the most primitive basaltic rocks (ankaramites) of the Eyjafjallajökull volcano, and the third investigates basalt fractionation processes within the Hafnarhraun pāhoehoe lava lobe.

The sub-Icelandic mantle is evidently heterogeneous in composition. Yet olivine major and minor element compositions in Iceland basalts typically concur with common mantle lherzolite as the source of magmas, with the only potential exceptions being the basalts of Eyjafjallajökull and Vestmannaeyjar volcanic systems in South Iceland. These South Iceland basalts have forsterite-rich olivine with relatively high Ni and low Mn contents, together with low Sc and V and high Cr, Ti, Zn, Cu and Li contents. Elevated Ni and low Mn in olivine have been attributed to olivine-free pyroxenitic mantle source; however, the South Iceland olivine compositions are best explained by the effect of comparatively high-pressure (P_{final}>1.4 GPa) and high-temperature melting of somewhat enriched olivine-bearing mantle. I conclude this because (i) elevated Ni and low Mn in olivine can also indicate deep, high-temperature, mantle melting, (ii) the abundances of Sc, V, Ti and Zn in the South Iceland olivine are compatible with low-degree partial melts of olivine-rich mantle, and (iii) melts of olivine-free pyroxenite are, according to recent models, easily consumed in reactions with subsolidus mantle peridotite and thus unlikely to migrate to the crust and crystallize olivine. The identified high-Ni/low-Mn olivine macrocrysts suggest final mantle equilibration depths greater than 45 km for South Iceland magmas, and imply effective mantle-to-surface magma transport.

Two Eyjafjallajökull ankaramite outcrops (Hvammsmúli and Brattaskjól), rich in olivine ($Fo_{81–90}$) and clinopyroxene ($Mg\#^{cpx}$ 78–90) macrocrysts (~30 vol%) in near equal amounts, have a specifically prominent "deep mantle source signature" (high-Ni/low-Mn) in olivine. To investigate the crustal storage conditions of these and other Eyjafjallajökull basaltic magmas, I analyzed olivine, clinopyroxene, spinel and melt inclusion compositions from these volcanic units. These analyzes revealed that the olivine-hosted spinel inclusions have exceptionally high $Cr\#^{spl}$ (52–80) and TiO_2 (1–3 wt%) and low Al_2O_3 (8–22 wt%) compared to typical chromian spinels in Iceland, in line with the postulated deep and enriched mantle source of the parental magmas. According to olivine-spinel oxybarometry, these spinels crystallized under a moderate oxygen fugacity (ΔlogFMQ 0–0.5). Furthermore, jadeite-in-clinopyroxene barometry indicates clinopyroxene crystallization at a rather low pressure (1.7–4.2 kbar; external precision ±1.4 kbar), implying a magma storage depth of 10.7±5 km. Additionally, clinopyroxe-liquid, olivine-liquid and liquid only thermometry gives varying crystallization temperatures of 1120–1195 °C, 1136–1213 °C and 1155–1222 °C, respectively, for

the compositionally diverse macrocrysts. The scarcity of macrocryst plagioclase and trends in clinopyroxene compositions indicate that the mid-crustal crystallizing assemblage was olivine and clinopyroxene, and plagioclase fractionated later. Diffusive re-equilibration in Brattaskjól olivine grains suggests that this crystal assemblage mobilized and erupted from its storage within a few weeks. To conclude, the Brattaskjól and Hvammsmúli crystal cargoes are agitated wehrlitic or plagioclase-wehrlitic mushes from the mid-crust that ascended to the surface relatively rapidly.

Basaltic lavas are practically never primitive mantle melts owing to fractional crystallization in the crust, which, at low pressure, may be aided by volatile exsolution. Deciphering magma fractionation processes from solidified crustal intrusions is hampered by their often complex emplacement history. The emplacement of pāhoehoe lavas, however, is simpler and well understood, and hence I investigated the mechanisms of basalt fractionation from a differentiated pāhoehoe lava lobe in Hafnarhraun lava flow field. Here, volatile exsolution had facilitated separation of basaltic residual melts to form three types of melt segregations: vesicle cylinders (VC) in the core of the lobe and two types of horizontal vesicle sheets (HVS1 and HVS2) in the upper part of the lobe. Interestingly, the VC do not match chemically with the modelled residual melts of the lobe, and their formation seems to have included two stages: volatile-aided melt separation from crystallizing base of the lobe and later contamination by primitive macro- and microphenocrysts in the lava core. HVS1, which resemble VC, were formed as the ascending VC diapirs accumulated to the upper solidification front of the lava lobe. HVS2, in turn, are distinctly evolved in compositions compared to other units in the lobe and were formed as highly fractionated residual melts seeped to voids in the upper crust of the lobe. Processes analogous to segregation formation at Hafnarhraun may contribute to genesis of evolved basalts and silicic rocks in shallow magmatic systems.

Overall, my work highlights the exceptional nature of South Iceland among other volcanically active regions in Iceland. Furthermore, analyses of the Hafnarhraun pāhoehoe lava reveal the processes of melt segregation formation in pāhoehoe lava lobes. I hope future research will expand on these findings, further resolving the nature of mantle melting below South Iceland and the significance of volatile-aided processes in crustal magma differentiation.

Tiivistelmä

Tämä väitöskirja käsittelee Islannin basalttisten laavojen syntyä ja kehitystä. Väitöskirjan ensimmäisessä osassa käytän laavoissa esiintyvien oliviinihajarakeiden koostumuksia Islannin alaisen maapallon vaipan sulamisolosuhteiden indikaattorina, toisessa selvitän Eyjafjallajökull-tulivuoren ankaramiitti-laavojen purkautumista edeltäviä säilytysolosuhteita maankuoressa, ja kolmannessa tutkin pāhoehoe-laavan fraktioitumisprosesseja Hafnarhraun-laavakentällä.

Maapallon vaippa Islannin alla on todennäköisesti koostumukseltaan vaihteleva. Tästä huolimatta oliviinihajarakeiden koostumus Islannin basalteissa on tyypillisesti yhtenevä vain lherzoliittisen magmojen vaippalähteen kanssa. Tähän ainoa poikkeus ovat eteläisen Islannin Eyjafjallajökull- ja Vestmannaeyjar-tulivuorten laavoissa esiintyvät oliviinihajarakeet, joissa on korkea nikkeli- ja matala mangaanipitoisuus, mutta myös alhainen skandium ja vanadium, sekä korkea kromi, titaani, sinkki, kupari ja litium. Vaikka oliviinin korkea nikkeli- ja matala mangaanipitoisuus voidaan nähdä oliviinista köyhän pyrokseniittiseen vaipan indikaattorina, eteläisen Islannin poikkeavat oliviinikoostumukset selittyvät parhaiten vaipan syvällä sulamisella korkeassa lämpötilassa. Esitän näin sillä (i) korkea nikkeli ja matala mangaani oliviinissa voi olla myös seurausta vaipan korkeasta sulamislämpötilasta, (ii) Sc-, V-, Ti- ja Zn-pitoisuudet eteläisen Islannin oliviinihajarakeissa viittaavat oliviinirikkaaseen vaipan lähteeseen, ja (iii) uusimpien vaipan sulamisen mallien mukaan pyrokseniittivaipan sulat reagoivat helposti ympäröivän lherzoliittivaipan kanssa ja näin ne tuskin säilyvät muuttumattomina noustessaan kohti maapallon kuorta. Löydetyt korkean nikkelin ja matalan mangaanin oliviinihajarakeet viittaavat siihen, että eteläisen Islannin magmat tasapainottuvat vaipan lähteen kanssa yli 45 km syvyydessä ja nousevat tämän jälkeen tehokkaasti litosfäärin läpi.

Erityisen voimakas syvän vaipan sulamisen signaali (korkea nikkeli ja matala mangaani oliviinissa) havaittiin kahdesta ankaramiitti-laavasta (Hvammsmúli ja Brattaskjól) Eyjafjallajökull-tulivuoren rinteiltä. Selvittääkseni näiden laavojen purkautumista edeltävät säilytysolosuhteet maankuoressa, analysoin niistä oliviini-, klinopyrokseeni-, spinelli- ja sulasulkeumakoostumuksia. Havaitsin, että oliviinihajarakeiden spinellisulkeumilla on poikkeuksellisen korkea $Cr\#^{spl}$ (52–80) ja TiO_2 (1–3 m–%) sekä matala Al_2O_3 (8–22 m–%) verrattuna Islannista aiemmin analysoituihin Cr-spinelleihin, mikä on yhtenevää näiden ankaramiittien oletetun syvän ja rikastuneen vaippalähteen kanssa. Oliviini-spinelli oxybarometrian mukaan spinellit kiteytyivät hapen fugasiteetin ollessa ΔlogFMQ 0–0,5. Klinopyrokseenin jadeiittipitoisuuteen perustuva barometria puolestaan indikoi verrattain matalaa (1,7–4,2 kbar; metodin tarkkuus ±1,4 kbar) klinopyrokseenien kiteytymispainetta, mikä vastaa 10,7±5 km syvyyttä maapallon kuoressa. Klinopyrokseenin, oliviinin ja sulan koostumukseen perustuvat termometrit antavat hajarakeille vaihtelevia kiteytymislämpötiloja: 1120–1195 °C, 1136–1213 °C ja 1155–1222 °C. Hajarae plagioklaasin harvinaisuus ja klinopyrokseenihajarakeiden koostumuksellinen vaihtelu osoittavat, että keskikuoressa kiteytyvä mineraaliseurue koostui oliviinista ja klinopyrokseenista, ja plagioklaasi kiteytyi magmoista myöhemmin. Näin ollen tutkittujen ankaramiittien hajarakeet ovat luultavasti peräisin keskikuoren wehrliittisistä tai plagioklaasi-wehrliittisistä kidepuuroista.

Näihin kidepuuroihin tunkeutuvat magmat nostattivat hajarakeet muutaman viikon sisällä maanpintaan, mikä voidaan arvioida diffusiivisen tasapainottumisen määrästä Brattaskjól-ankaramiitin oliviinihajarakeiden vyöhykkeellisyydessä.

Pintaan purkautuvat basalttiset laavat eivät käytännössä koskaan enää edusta vaipan sulia, sillä fraktioiva kiteytyminen on muuttanut niiden koostumusta niiden noustessa maankuoren läpi. Magman fraktioitumisprosessien tutkiminen maankuoren plutoneista on haastavaa niiden usein monimutkaisen muodostumishistorian vuoksi. Pāhoehoe-laavojen asettuminen on yksinkertaisempaa ja näin ollen tutkin basalttisen magma fraktioitumisprosesseja pāhoehoe-laavapatjasta Hafnarhraun-laavakentällä. Tutkitussa laavassa volatiilien erottuminen magmasta oli edesauttanut jäännössulien erottumista ja muodostanut kolmen tyyppisiä segregaatiosulia laavan sisään: rakkulapiippuja (VC) pāhoehoe-laavan ytimeen ja kahden tyyppisiä horisontaalisia rakkulapatjoja (HVS1 ja HVS2) laavapatjan yläosiin. VC koostumukset eivät vastannut laavan mallinnutettuja jäännössulia, mutta ne voitiin selittää kaksivaiheisella syntyhistorialla, jossa VC ensin erottuvat volatiiliavusteisesti isäntämagmasta laavan pohjaosissa ja tämän jälkeen niihin kertyy oliviini- ja plagioklaasikiteitä laavapatjan keskiosissa. HVS1 muodostuivat, kun nousevat VC levittäytyivät laavan kiteytyvän yläkuoren alapintaa vasten, ja HVS2 ovat pitkälle fraktioituneita isäntälaavan jäännösulia, joita tihkui laavan yläkuoreen muodostuneisiin aukkoihin ja rakoihin. Hafnarhraun pāhoehoe-laavan segregaatiosulien erottumista muistuttavat prosessit saattavat johtaa kehittyneiden basalttisten magmojen muodostumiseen maanpinnan läheisissä magmasäiliöissä.

Väitöskirjatutkimuksessani paljastui eteläisen Islannin ainutlaatuisuus verrattuna Islannin muihin magmaattisesti aktiivisiin alueisiin. Tämän lisäksi Hafnarhraun pāhoehoe laava osoitti volatiilien merkityksen sulasegregaatioiden synnyssä. Toivon, että löydöksieni päälle rakennetaan uutta tutkimusta, joka vie ymmärrystämme eteenpäin selvittäen eteläisen Islannin magmojen vaippalähteen luonnetta ja volatiilien merkitystä magmojen fraktioitumisessa.

Ágrip

Í þessari ritgerð er ljósi varpað á uppruna basaltkviku á Íslandi með þremur rannsóknarþemum. Í fyrsta þemanu er snefilefnainnihald ólívíndíla notað til að skýra hvaða skilyrði ríkja við hlutbræðslu möttulsins undir Íslandi. Í öðru þemanu er stuðst við jarðefnafræðilega hita- og þrýstimæla til þess að meta eiginleika kvikuhólfa/-þróa sem innihalda frumstæða basaltkviku (þ.e. ankaramít) í skorpunni undir Eyjafjallajökli. Þriðja þemað varðar þróunarferli basaltbráðar í helluhraunssepa í Hafnarhrauni við Þorlákshöfn.

Möttulinn undir Íslandi er að samsetningu misleitur. Samt samræmist aðal- og snefilefnasamsetning ólívíndíla í íslensku basalti kviku sem á uppruna sinn að rekja til hlutbræðslu á venjulegum lherzólítmöttli. Hugsanleg undantekning frá þessari reglu er basaltkvikan sem kemur upp í eldstöðvakerfunum Eyjafjallajökli og Vestmannaeyjum, sem innihalda mjög forsterítríka ólívíndíla með tiltölulega háan Ni-styrk og lágan Mn-styrk, ásamt lágum styrk Sc og V og háum styrk Cr, Ti, Zn, Cu og Li. Þrátt fyrir að hár Ni-styrkur og lágur Mn-styrkur í frumstæðum ólívíndílum sé gjarnan rakinn til kviku sem myndast við hlutbráðnun á ólívínlausum pyroxenítmöttli, þá er samsetning umræddra ólívíndíla best skýrð með háhitabráðnun á auðguðum, ólívínríkum perídótítmöttli við háan þrýsting (P_{final} > 1,4 GPa). Ég dreg þessa ályktun vegna þess að (i) hár Ni-styrkur og lágur Mn-styrkur í ólívíni samræmist einnig bráðnun við háan hita djúpt í möttlinum, (ii) tiltölulega hár styrkur Sc, V, Ti og Zn í ólívíndílunum er í samræmi við litla hlutbráðnun á ólívínríkum möttli, og (iii) samkvæmt nýjustu líkönum hvarfast pýroxenítbráð auðveldlega við möttulperidótít og því ólíklegt að slík bráð komist upp í jarðskorpuna og kristalli ólívín. Þessi hái styrkur Ni og lágur styrkur Mn í ólívíndílunum bendir til þess að kvikan hafi síðast verið í jafnvægi við möttulefnið á meira en 45 km dýpi og að kvikan hafi flust hratt frá möttli til yfirborðs.

Tvær ankaramítmyndanir í Eyjafjöllum, Hvammsmúli og Brattaskjól, sem auðugar eru af ólívíndílum ($Fo_{81–90}$) og klínópýroxendílum ($Mg\#^{cpx}$ 78–90) (~ 30%), nokkurn veginn í sama magni, sýna merki um uppruna djúpt í möttlinum, þ.e. hátt Ni-magn / lágt Mn-magn í ólívíndílunum. Efnasamsetning ólívíns, klínópýroxens, spínils og bráðarinnlyksna var greind í sýnum frá þessum myndunum til þess að meta dýpi kvikuþróa þar sem þessar kvikur safnast fyrir í skorpunni fyrir gos. Þessar greiningar sýna að spínilkristallarnir, sem eru til staðar sem innlyksur í ólívíndílum, hafa óvenju hátt $Cr\#^{spl}$ (52–80) og mikið af TiO_2 (1–3 þ.%) og lítið af Al_2O_3 (8–22 þ.%) í samanburði við dæmigerða krómspínla í íslensku basalti. Þetta er í takt við ályktunina um djúpstæðan uppruna móðurkvikunnar frá auðguðum möttli. Samkvæmt ólívín-spínil súrefnisþrýstingsmælinum kristölluðust þessir spínlar við hóflegan súrefnisstyrk (ΔlogFMQ 0–0,5). Jafnframt bendir þrýstimælir sem byggir á magni jaðeítþáttar í klínópýroxeni til að kristöllun klínópýroxens hafi átt sér stað við frekar lágan þrýsting (1,7–4,2 ± 1,4 kbar), sem gefur til kynna 10,7 ± 5 km dýpi fyrir kvikuþróna. Að auki gefa hitamælar fyrir klínópýroxen-gler, ólívín-gler og gler eingöngu mismunandi kristöllunarhitastig fyrir hinar mismundi gerðir fasa, nefnilega 1120–1195 °C, 1136–1213 °C og 1155–1222 °C. Lítið magn plagíóklasdíla ásamt samsetningu klínópýroxendílanna bendir til þess að þessar kvikur hafi kristallað ólívín og klínópýroxen í kvikuþrónni og myndun plagíóklasdíla hafist síðar. Líkanreikningar á efnasveimi í ólívíni frá Brattaskjóli bendir til að þessi dílafarmur hafi farið að stað úr geymslurýminu og borist til yfirborðs í eldgosi innan nokkurra vikna. Niðurstaðan er að dílafarmurinn í Brattaskjóli

og Hvammsmúla sé að uppruna kristalríkur massi í miðskorpunni með steindafylki wehrlíts eða plagíóklas-wehrlíts sem reis tiltölulega hratt til yfirborðs.

Basalthraun eru nær aldrei með sömu samsetningu og frumstæðar möttulbráðir vegna hlutkristöllunar sem á sér stað í jarðskorpunni, en hlutkristöllunin getur við lágan þrýsting orðið fyrir áhrifum af aðskilnaði gastegunda. Erfitt getur verið að greina áhrif þróunarferla í kviku með því að skoða storknuð innskot vegna flókinnar sögu þeirra oft á tíðum. Hins vegar er myndun helluhrauna vel skilin og hef ég því rannsakað kvikuþróunarferli basalts með því að skoða þróaðan helluhraunssepa í Hafnarhrauni. Í þessu tilfelli átti aðskilnaður gass þátt í aðskilnaði afgangsbráðar með samsetningu basalts. Bráðaraðskilnaðurinn var af þrennu tagi: blöðrusívalningar (VC) í kjarna hraunsepans og tvær gerðir láréttra blöðrulaga (HVS1 og HVS2) í efri hluta sepans. Áhugavert er að efnasamsetning VC fellur ekki að líkanreikningum fyrir sepann og myndun þeirra virðist hafa orðið í tveimur þrepum: bráðaraðskilnaður með hjálp gass í botni sepans þar sem kristöllun átti sér stað og síðar mengun af frumstæðum stór- og smádílum í kjarna hraunsins. HVS1 líkjast VC og mynduðust þegar VC-sívalningar risu og söfnuðust fyrir á storknunarmörkum hraunsepans. Hins vegar eru HVS2 greinilega þróaðir í samanburði við hinar gerðirnar í sepanum og mynduðust við að mjög þróaðar afgangsbráðir seytluðu í holrými í efri skorpu sepans. Ferli lík þeim sem mynduðu afgangsbráðirnar í Hafnarhrauni gætu komið við sögu við myndun þróaðs basalt og súrs bergs í grunnstæðum kvikukerfum.

Heilt yfir litið þá sýna rannsóknir mínar hversu einstakt Suðurgosbeltið er meðal virkra gosbelta á Íslandi. Þá hafa rannsóknirnar á Hafnarhrauni leitt í ljós ferli bráðaraðskilnaðar í helluhraunssepum. Ég vona að framtíðarrannsóknir muni byggja á þessum uppgötvunum og leiða til betri skilnings á eðli möttulbráðnunar undir Suðurlandi og því hversu mikilvægt gas er fyrir kvikuþróunarferli í skorpunni.

Acknowledgements

I want to thank my supervisors Thorvaldur (Thor) Thordarsson and Tapani Rämö. Thor kindly took me under his wing when I decided to start a PhD in Iceland. He encouraged me to start on this path and supported me through thick and thin. Tapani, in turn, was invaluable for finishing this project with his deadlines and tireless supervision, especially during the last two years. Tapani was also the first, already eons ago, who got me interested in igneous petrology.

Secondly, my life-long gratitude goes to Enikő Bali and Guðmundur H. Guðfinnsson who contributed immensely to two of my thesis manuscripts and helped me back on track when my thesis topic changed in 2016. Without their help and vision, my thesis would not be as it is today, and I may have never become obsessed over olivine macrocrysts.

Furthermore, I thank my co-authors Tobias Fusswinkel, Maren Kahl, Quinten van der Meer and Pasi Heikkilä who helped me during these years. My gratitude also goes to the following, who aided me on the thesis research: Jussi Heinonen, Sanni Turunen, Sæmundur Ari Halldórsson, Matthew Pankhurst, David Neave, Leó Kristjánsson, Atli Hjartarson, Robert Askew and Maja Bar Rasmussen.

Then I want to mention Rikke Pedersen who was the boss during my years working for the Nordic Volcanological Center. She was there when needed.

Others were there also, and as they hang around long enough, they became friends. In fact, friends are likely the best thing I got from this endeavor they call a PhD. It boggles my mind how many good moments we have shared. I kid you not, once a lava tornado nearly roasted some of us. As listing you all by name would be too wordy, I announce the following: greatest thanks to the First-response team Holuhraun, Petrosquad, Vesturbæjarlaug swimmers, Da running club, Flóki and Folda, and Room 227.

This work would have not been possible without the support of my family: the one in Alavus, the one in Njarðvík, and the one in Espoo. This thesis is dedicated to Gadidjah and Aaron.

Contents

Abstract 3
Tiivistelmä 5
Ágrip 7
Acknowledgements 9
List of original publications 11
Author's contribution to the publications 11
Abbreviations 12
List of figures 13

1 Introduction 14
1.1 Aims, motivation and outcome 14
1.2 Anatomy of the thesis 14
2 Basaltic magmatism in Iceland 15
2.1 The volcanic setting 15
2.2 Mantle origin of Iceland basalt 17
2.3 Basalt differentiation 18
2.4 Storage of magmas in the Iceland crust 20
3 Sampling and laboratory analysis of rocks and minerals 20
3.1 Samples 20
3.2 XRF 21
3.3 EPMA 21
3.4 LA-ICP-MS 22
3.1 EBSD 22
4 Numerical modelling 23
4.1 Major, minor and trace elements in olivine as a mantle proxy 23
4.2 Thermodynamic modelling of melting and crystallization 23
4.3 Thermobarometry—probing the crystallization conditions of minerals 24
4.4 Kinetic modelling of diffusion time scales 26
5 Review of original papers 27
5.1 PAPER I 27
5.2 PAPER II 28
5.3 PAPER III 29
6 Discussion 30
6.1 Dynamics of mantle melting (PAPER I) 30
6.2 Magma storage and crystallization in the South Iceland crust (PAPER II) 33
6.3 Insights to basalt differentiation from the Hafnarhraun lava lobe (PAPER III) 35
7 Conclusions and future directions 36
References 36
APPENDICES I–IV 44
PAPERS I–III

List of original publications

This thesis is based on the following publications:

I Nikkola P., Guðfinnsson G.H., Bali E., Rämö O.T., Fusswinkel T., Thordarson T. 2019. Signature of deep mantle melting in South Iceland olivine. Contributions to Mineralogy and Petrology 174:43.

II Nikkola P., Bali E., Kahl M., Quinten H. A. van der Meer, Rämö O.T., Guðfinnsson G.H., Thordarson T. 2019. Mid-crustal storage and crystallization of Eyjafjallajökull ankaramites, South Iceland. Jökull 69:77–96.

III Nikkola P., Thordarson T., Rämö O.T., Heikkilä P. 2019. Formation of segregation structures in Hafnarhraun pāhoehoe lobe, SW Iceland: a window into crystal–melt separation in basaltic magma. Bulletin of Volcanology 81:70.

The publications are referred to in the text by their roman numerals.

Author's contribution to the publications

I The original idea for the research came from EB and GHG. Collection of the samples was done by PN, EB and GHG. PN conducted all microanalyses and related laboratory work with the guidance of GHG and TF. PN is fully responsible for all geochemical modelling and he wrote the manuscript with contributions from the co-authors.

II PN, EB, MK and GHG planned the study. PN and QM did the microanalyses of mineral compositions, EB performed the melt inclusion experiments and analyses, and MK conducted the EBSD analyses of olivine crystallographic orientation. PN did the thermobarometric and diffusion modelling and wrote the manuscript with input from the co-authors.

III The idea of the study came from TT and was developed by PN. PN is fully responsible of all fieldwork, sampling, geochemical modelling and interpretations. He conducted all microanalyses of mineral phases and performed the whole rock analyses with the guidance of PH. PN wrote the manuscript with input from the co-authors.

Abbreviations

An	anorthite
CaTs	calcium Tschermak component
cf.	*confer*
$Cr\#^{spl}$	chromium number in spinel
D	distribution coefficient
DiHd	diopside hedenbergite
EBSD	electron backscatter diffraction
ED	energy dispersive
EnFs	enstatite ferrosilite
EPMA	electron probe microanalyzer
EVZ	Eastern Volcanic Zone
e.g.	*exempli gratia*
F	degree of partial melting
Fo	forsterite
fO_2	oxygen fugacity
G	Gibb's free energy
HVS	horizontal vesicle sheets
i.e.	*id est*
ICP–MS	inductively coupled plasma mass spectrometer
Jd	jadeite
KDE	kernel density estimation
Kd^{Mg-Fe}(cpx–liq)	Mg/Fe exchange coefficient between clinopyroxene and melt
LAB	lithosphere-asthenosphere boundary
LA–ICP–MS	laser ablation inductively coupled plasma mass spectrometry
LLD	liquid line of decent
Ma	million years (mega-annum) before present
$Mg\#^{cpx}$	magnesium number of clinopyroxene
$Mg\#^{liquid}$	magnesium number of liquid
Moho	Mohorovičić discontinuity
MORB	mid-ocean ridge basalt
MIB	Mid-Iceland Belt
NVZ	Northern Volcanic Zone
OIB	ocean island basalt
ÖVZ	Öræfajökull Volcanic Zone
P	pressure
ppm	parts per million
RVZ	Reykjanes Volcanic Zone
SEM	secondary electron microscope

SEVZ	Southern tip of the Eastern Volcanic Zone
SISZ	South Iceland Seismic Zone
SVZ	Snæfellsness Volcanic Zone
T	temperature
VC	vesicle cylinders
WD	wavelength dispersive
WVZ	Western Volcanic Zone
X_{px}	relative contribution of olivine-free pyroxenite-derived melt
XRF	X-ray fluorescence
1SEE	one standard error of estimate
ΔlogFMQ	logarithmic deviation from the Fayalite-Magnetite-Quartz oxygen buffer

List of figures

Fig 1 *Geological map of Iceland and the sample locations*, page 16

Fig 2 *Illustration of the mantle melting regime in rift and flank zone volcanism in Iceland*, page 19

Fig 3 *Diffusion chronometry: modelling of the time of diffusive re-equilibration in minerals*, page 27

Fig 4 *Hafnarhraun pāhoehoe lava lobe and its key internal structures*, Page 30

Fig 5 *The input of mantle pyroxenite derived partial melts to Iceland basalts as indicated by olivine compositions,* page 31

Fig 6 *Conceptual model of magma storage below Eyjafjallajökull volcano*, Page 34

1 Introduction

1.1 Aims, motivation and outcome

The overarching aim of my thesis is to improve the understanding of basaltic magma genesis in Iceland. This is a broad goal, as the origin of basalts is one of the core topics of igneous petrology and Iceland is a classical locus of basalt research. Nonetheless, I have tackled this aim with three separate projects that each have independent goals as follows:

(i) To evaluate the variability in olivine minor and trace element contents in various geotectonic localities in Iceland and use this to infer compositional heterogeneity in the mantle source of Icelandic basalts (PAPER I).

(ii) To estimate conditions and timescales of the crustal storage of macrocrysts in Eyjafjallajökull ankaramites for a model of crustal magma transport in South Iceland (PAPER II).

(iii) To study a differentiated pāhoehoe lava lobe to decipher and describe mechanisms of crystal-melt separation in a typical olivine tholeiite basalt (PAPER III).

Investigating these topics of basaltic magma genesis is important, because they are essential for our understanding of the workings of the Earth's upper mantle and crust. Furthermore, estimating the conditions of crustal magma storage below active volcanoes is required for identifying the mechanisms leading to possibly hazardous volcanic eruptions. In the inners of our planet, intricacies of silicate partial melting and crystallization determine how material circulates and behaves, and Iceland is a good location to study these processes.

The most significant outcome of my thesis is the identification of an anomalous, in the context of previous Iceland data, deep mantle melting signature in olivine from South Iceland volcanic rocks (PAPER I). PAPER II shows that the clinopyroxene macrocrysts of Eyjafjallajökull ankaramites crystallized at surprisingly low mid- and upper-crustal pressures (3.0±1.4 kbar). This suggests that early clinopyroxene fractionation from primitive South Iceland magmas can occur shallower in the crust than previously thought. Furthermore, the Hafnarhraun pāhoehoe lava lobe (PAPER III) revealed the mechanisms of crystal-melt separation in this differentiated basalt, potentially analogous to mechanisms occurring in shallow crustal intrusions, thus providing valuable insights into basalt magma genesis.

1.2 Anatomy of the thesis

In PAPER I, I investigate mantle melting below Iceland by analyzing major, minor and trace element compositions of primitive olivine crystals from various tectonic settings in Iceland (eight sampling locations and 482 analyzed olivine grains in total). Olivine analyses were performed with high-precision EPMA and LA-ICP-MS, and the results were compared to numerical models of mantle melting and olivine crystallization. Olivine crystals are a valuable proxy of the mantle mode (i.e., rock type) and melting conditions, as they are the first phase to crystallize from a primitive basaltic magma, and thus record a nearly unmodified, initial composition of the mantle-derived partial melt. Knowledge on the composition of these near-primary mantle melts can be further used to infer the nature of their mantle source.

In addition to mantle processes, my thesis explores how basaltic magmas reside and differentiate in the Earth's crust. This—crustal storage of magmas—is the topic of PAPER II, for which I analyzed clinopyroxene, olivine, spinel and melt inclusions in the most primitive rocks of Eyjafjallajökull to determine at what pressure and temperature these crystals crystallized. Compositional analyses were performed with EPMA, and pressure and temperature estimates were de-

rived using the most recent thermobarometric models. In addition, I analyzed compositional zonation patterns in olivine crystals, formed by magma mixing-induced growth and subsequent solid-state diffusion, to estimate how long these crystals spent in the magmatic system after the magma-mixing event. The necessary crystallographic orientation data for these diffusion models were acquired with EBSD.

PAPER III is a thorough description of a differentiated pāhoehoe lava lobe. It focuses on the question of how residual melts of the partly crystalline lava separated to form evolved units (melts segregations) within the lava lobe. Composition of whole-rock samples and main minerals in the pertinent units within the lava lobe were analyzed using WD-XRF and EPMA. Pāhoehoe lavas are useful for this type of a study, as they are modest in size, crystallize at atmospheric pressure, and have a relatively simple emplacement mechanism in comparison to exposed crustal basaltic intrusions.

2 Basaltic magmatism in Iceland

2.1 The volcanic setting

Basaltic magmas are partial melts of the Earth's upper mantle. These melts have a low density in comparison to common mantle rocks; therefore, they ascend through Earth's upper layers and sometimes erupt as lava flows. At mid-ocean ridges, basalt differentiation and solidification generate the oceanic crust (Wilson, 1963). Ultimately, basaltic magmatism also contributes to the formation of continental crust, atmosphere and oceans, making Earth as we know it (Allègre et al., 1987; Hofmann, 1988).

Globally, Iceland is one of the most proficient producers of basaltic magma (Thordarson and Larsen, 2007). It is a volcanic island situated in the North Atlantic between the Eurasian and North-American lithospheric plates that diverge by a rate of 18–19 mm/year (Sigmundsson et al., 2018). This spreading is concentrated at rift zones, 50–100 km in width, which cross Iceland from southwest to northeast (Fig. 1). In the southern half of Iceland, there are two parallel rift zones, Eastern Volcanic Zone (EVZ) and Western Volcanic Zone (WVZ). Between these resides a crustal block, called the Hreppar Formation, which is bordered by the Mid-Iceland Belt (MIB) in the north and the South Iceland Seismic Zone (SISZ) in the south. SISZ, as the name suggests, is an earthquake-prone transform, and here lithospheric spreading is accommodated as a left-lateral shear in "bookshelf" type faulting (Einarsson, 2010). At its western extremity, the SISZ fuses with the WVZ, and this part of the plate boundary is the Reykjanes Volcanic Belt (RVB). Here, the plate boundary trends characteristically oblique (~30°) to the plate spreading direction (Clifton and Kattenhorn, 2006). The tectonic setting in the northern half of Iceland is generally simpler than in the south, featuring a single rift zone that accommodates all deformation: Northern Volcanic Zone (NVZ). In the northernmost Iceland, this simplicity is lost again, as NVZ converts to a complex transform zone—the Tjörnes Fracture Zone (TFZ)—that accommodates both right-lateral shear and extension (Stefansson et al., 2008).

Owing to magmatism focused at the spreading rifts, the age of the Iceland crust increases away from them (Fig. 1), such that the oldest rocks are at the eastern and western extremities of the island, being 12–13 Ma old at the eastern coast and 15–16 Ma in the northwest (Moorbath et al., 1968). This pattern is broken by volcanic flank zones (also called off-rift volcanic zones), where magmas erupt off-rift and accumulate unconformably on older strata (Fig. 1). The three major flank zones are Snæfellsness

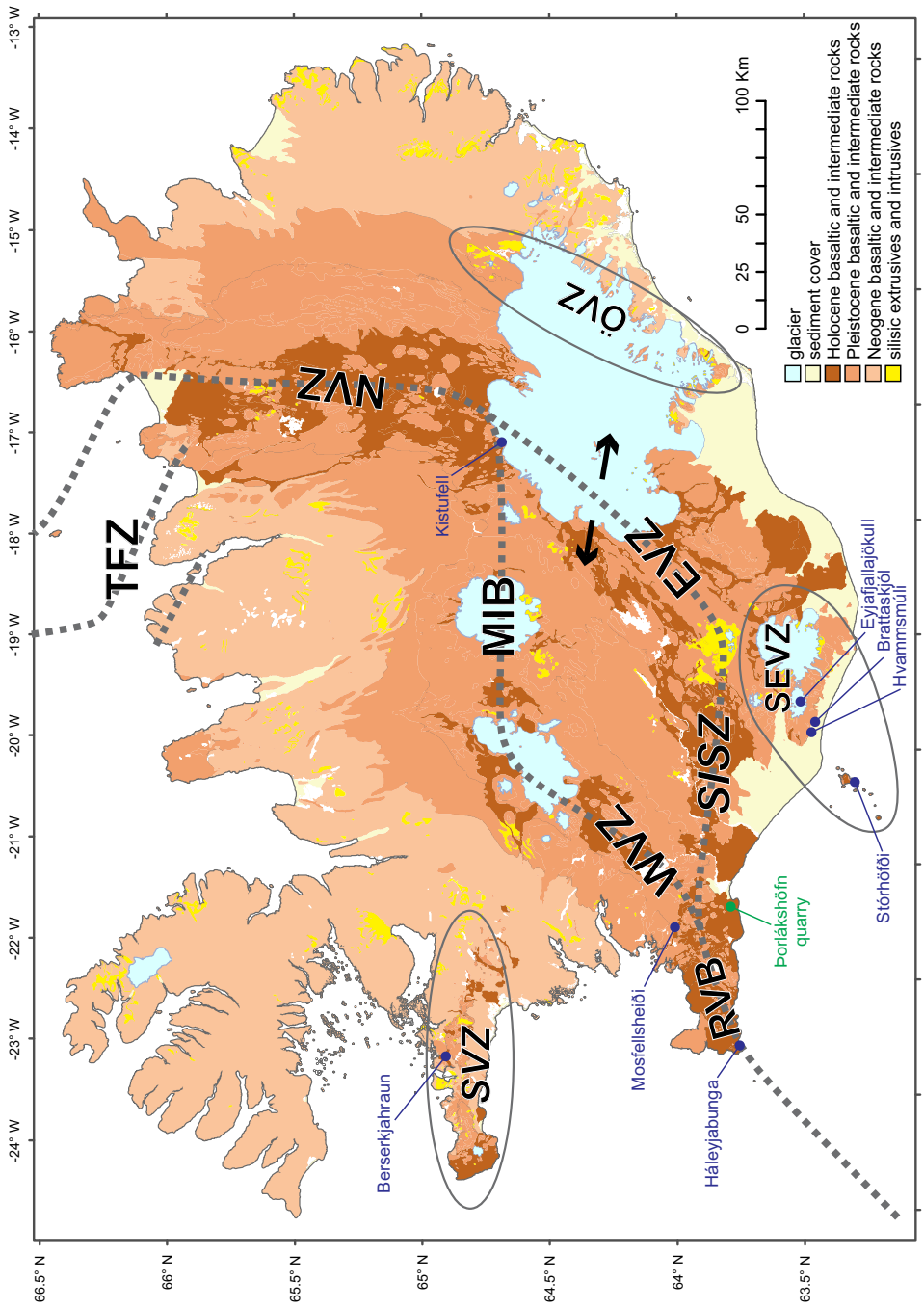

Figure 1. Geological map of Iceland. Stippled line marks the active plate boundary. Arrows show the direction of crustal spreading. Ovoids delineate the volcanic flank zones (i.e., off-rift zones) with little or no rifting. Pertinent sampling locations of the thesis are marked. Acronyms: SVZ = Snæfellsness Volcanic Zone, RVB = Reykjanes Volcanic Belt, WVZ = Western Volcanic Zone, SISZ = South Iceland Seismic Zone, MIB = Mid-Iceland Belt, TFZ = Tjörnes Fracture Zone, EVZ = Eastern Volcanic Zone, NVZ = Northern Volcanic Zone, ÖVZ = Öræfajökull Volcanic Zone.

Volcanic Zone (SVZ), Southern tip of the Eastern Volcanic Zone (SEVZ) and Öræfajökull volcanic zone (ÖVZ). The reasons behind the magmatism in off-rift volcanic zones are not completely clear. However, SVZ has been interpreted as a remnant of the now extinct Snæfellsnes-Skagi rift segment, and as such a zone of weakness in the crust (Hardarson et al., 1997), while SEVZ has been suggested to be the off-rift tip of the southward propagating EVZ (Oskarsson et al., 1982). Furthermore, ÖVZ has been suggested to be a recently-developed locus of rifting (Hards et al., 2000) parallel to EVZ. Of the volcanic flank zones, SEVZ has been the most active during historical times (Thordarson and Larsen, 2007).

92 volume% of the Iceland magmas erupted in the Holocene have been basalts (Thordarson and Larsen, 2007), and silicic rocks are a minority in the rock record (Fig. 1). Basalts of the rift zones are olivine tholeiite or tholeiite, whereas basalts erupted from off-rift volcanoes tend to be alkali basalts or so-called transitional alkali basalts, meaning that they plot close to the alkalic-tholeiitic transition on a TAS diagram (see Jakobsson, 1972; Jakobsson et al., 2008). This compositional variation is likely due to varying mantle melting conditions during the genesis of these basalts.

2.2 Mantle origin of Iceland basalts

Abyssal peridotites, ophiolites and mantle xenoliths indicate that the Earth's upper mantle is dominantly composed of lherzolite with olivine, pyroxenes, and spinel or garnet as the dominant phases (e.g., Green and Ringwood, 1963, 1967; McDonough and Sun, 1995). Basaltic lavas, although nearly never primary partial mantle melts (O'Hara, 1968), typically conform as fractionated partial melts of mantle lherzolite, as shown by the plethora of melting experiments and numerical models (e.g., Green and Ringwood, 1967; Langmuir et al., 1977; Jaques and Green, 1980; Baker and Stolper, 1994).

The sub-Icelandic mantle melts in response to plate spreading induced upwelling and decompression. Additionally, it has been suggested that Iceland is underlain by a hot mantle plume (Schilling, 1973), which increases the melting rate at least in central Iceland (Maclennan et al., 2001a). Icelandic basalts commonly have an "enriched" isotopic signature with high $^{87}Sr/^{86}Sr$, $^{206}Pb/^{204}Pb$, $^{3}He/^{4}He$ and low $^{143}Nd/^{144}Nd$ compared to MORB (Hart et al., 1973; Sun and Jahn, 1975), although some basalts also reveal a depleted signature—with low $^{87}Sr/^{86}Sr$ and high $^{143}Nd/^{144}Nd$—distinct from MORB (e.g., Fitton et al., 1997; Thirlwall et al., 2004b). This compositional deviance from MORB is typically seen indicative of the presence of trace element enriched and undegassed mantle below Iceland brought up by the mantle plume (Chauvel and Hémond, 2000; Kokfelt et al., 2006; Harðardóttir et al., 2018), although alternative views do also exist (e.g., Hole and Natland, 2019). Further evidence for the Iceland plume comes from seismic tomography that indicates a low-velocity zone below Iceland, interpreted to represent the tail of the ascending plume (e.g., Wolfe et al., 1997; French and Romanowicz, 2015). Moreover, petrological thermometry suggests a hot mantle beneath Iceland, with estimated mantle potential temperatures of 1430–1630 °C compared to 1250–1400 °C for typical Mid-Oceanic Ridges (White and McKenzie, 1989; Mckenzie and O'Nions, 1991; Maclennan et al., 2001a; Putirka, 2008a, 2016; Brown and Lesher, 2014; Shorttle et al., 2014; Herzberg and Asimow, 2015; Jenkins et al., 2016).

When ascending mantle melts in response to plate spreading, it melts over a pressure (P) range, such that the degree of partial melting (F) progressively increases with lowering pressure (see Langmuir and Forsyth, 2007; and references therein). This induces variation in generated partial melt compositions, such that alkali basalts are produced at higher P and lower F, and tholei-

itic to picritic melts form at higher F and lower P. Some variation in basalt compositions is also derived from mantle heterogeneity. In Iceland, this is indicated by correlation in incompatible trace elements and long-lived radiogenic isotopes in basalts (Zindler et al., 1979; Hemond et al., 1993; Chauvel and Hémond, 2000; Kokfelt et al., 2006), which suggests that the enriched and fusible mantle components are distinct units from the depleted mantle and have been separated for hundreds of millions of years to attain their different isotopic signature. Because the fusibility of a mantle rock is governed by its major element composition (including water content), it can be assumed that these isotopically distinct and fusible mantle components are also their own rock types in the melting regime. Furthermore, the newest models indicate that the Icelandic mantle indeed needs to be modally heterogenous (Shorttle and Maclennan, 2011; Shorttle et al., 2014), as a minor (4–15%) contribution from olivine-poor mantle in the form of pyroxenite or pyroxenite-peridotite hybrid is required to generate the major and trace element compositional variation in erupted Iceland basalts.

The isotopically distinct and incompatible trace element-rich basalt compositions of the volcanic flank zones have been explained by contamination with lower crustal melts (Oskarsson et al., 1985; Steinthorsson et al., 1985), or by a lower degree of melting and greater average melting depth of compositionally heterogenous mantle (e.g., Furman et al., 1991a; Hemond et al., 1993; Kokfelt et al., 2006a). Although both processes are likely to have an effect on the genesis of flank zone basalts, the latter of these ideas, sketched in Fig. 2, has attained popularity, as it best explains the correlation between incompatible trace elements and isotopic enrichment in Iceland basalts (Sigmarsson and Steinthórsson, 2007; and references therein). Due to the thin lithosphere at the locus of rifting, mantle melting extends shallower and occurs over a greater pressure interval below rift zones compared to volcanic flank zones (green columns). Consequently, the degree of mantle melting is higher in rift zones, and the low-degree melts from fusible enriched mantle sources (yellow ellipses) are diluted by abundant shallow partial melts of depleted mantle. However, at volcanic flank zones, this dilution does not occur to the same extent, and thus the erupted magmas are (i) deep low-degree partial melts of the mantle, and (ii) more typically composed of partial melts of fusible, major and trace element-enriched mantle sources.

2.3 Basalt differentiation

After their formation in the sub-Icelandic mantle, the mantle melts need to transect 20 to 50 km of lithosphere (Darbyshire et al., 2000) before they erupt on surface. During this ascent, magmas accumulate at various depths and extended volumes of melts are stored and partially or completely crystallized. This crystallization is commonly fractional, meaning that the crystallizing mineral phases separate from the host melt soon after their formation, and thus the host melt composition alters due to the removal of elements by the fractionating crystal phases. This fractional crystallization is the key compositional modifier of magmas and so ubiquitous that completely non-fractionated magmas, so-called primary magmas, are rare on the surface of the Earth (O'Hara, 1968). Indeed, most erupted basaltic magmas in Iceland have already crystallized to reach the olivine + plagioclase cotectic (Hartley and Maclennan, 2018) or the phase assemblage olivine-plagioclase-clinopyroxene (Presnall and Gudfinnsson, 2011). The common order of fractionating mineral phases from reduced Icelandic tholeiitic magmas is olivine (±spinel), olivine + plagioclase and olivine + plagioclase + clinopyroxene (Herzberg, 2004). In addition, if the fractionating magma is sufficiently oxidized and

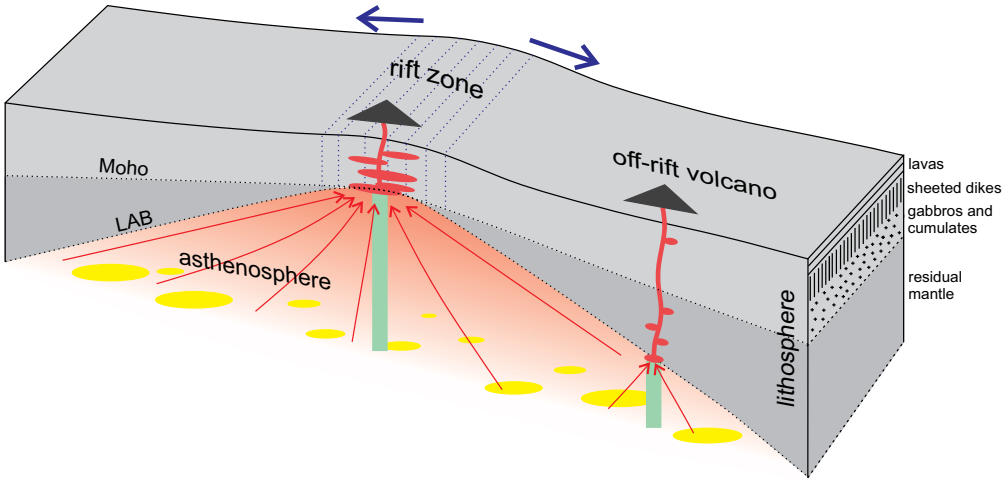

Figure 2. Conceptual model of mid-ocean ridge mantle melting and lithospheric structure. Yellow colored ovoids are modally and chemically enriched material in the mantle and triangles are volcanic edifices that tap the mantle melts. The strength of the red tone displays the degree of melting, fully red portions being dominantly molten. Red arrows are melt trajectories, and blue arrows illustrate the lithospheric spreading. The green bar shows the depth range of melting beneath rift and off-rift zones. Moho = Mohorovičić discontinuity, LAB = lithosphere-asthenosphere boundary.

poor in Ca and Al, and the crystallization pressure is sufficient, plagioclase crystallization may be suppressed to allow preferential crystallization of clinopyroxene after olivine (Presnall et al., 1978; Stolper, 1980; Presnall et al., 2002; Neave et al., 2019b).

Variably differentiated magmas from variable mantle sources are also prone to mix with each other during crustal storage. Primitive phenocryst phases commonly have melt inclusions that record high variability in trace element and isotopic contents. This variability, however, diminishes in more evolved phenocrysts. This has been interpreted as the result of 'concurrent mixing and crystallization' of magmas derived from various depths and sources from the mantle, which homogenizes magmas in crustal intrusions (Maclennan, 2008a, b; Neave et al., 2013). During this process, a large degree of the chemical variability inherited from polybaric mantle melting is lost.

Besides crystallization and mixing, intrusive magmas tend to interact with crustal rocks surrounding them. The stored magma can disaggregate rock fragments (xenoliths) or crystals (xenocrysts) and partially melt or resorb, i.e., assimilate, the surrounding crustal material. In Iceland, the limited compositional variability and the high melting point of the gabbroic crust limits this process and its effects on magma compositions, but isotopic and trace element studies nonetheless suggest that at least some Icelandic magmas have assimilated hydrothermally altered crust (Hemond et al., 1993; Brounce et al., 2012). In addition, Icelandic magmas commonly carry mineral cargoes that are not in chemical equilibrium with the carrier melt (Halldorsson et al., 2008; Thomson and Maclennan, 2013; Neave et al., 2014). These 'accumulated' non-equlibrium crystals can be xenocrysts: crystals not related to the host magma (Sollas, 1894), potentially derived by assimilation of fragments of crustal gabbro (e.g., Bédard, 1993). In addition, they can be antecrysts, co-genetic with the host magma but crystallized at an earlier evolutionary stage or in partial separation from the magma (Davidson et al., 2007). All these accumulated crystals affect the erupted magma compositions.

2.4 Storage of magmas in the Iceland crust

The storage of magmas in oceanic crust is evidently transcrustal, meaning that magmas reside in pockets in the Earth's crust at a range of depths (Maclennan et al., 2001b; Kelley and Barton, 2008; Maclennan, 2019; White et al., 2019). This view of multi-level magma storage conforms to detected seismicity during volcanic eruptions and sill emplacements (e.g., Tarasewicz et al., 2012; Greenfield and White, 2015), and to petrological barometry relying on final equilibration of a suite of magmatic liquids (Herzberg, 2004) and mineral-melt equilibrium in magmas (e.g., Neave and Putirka, 2017; Hartley and Maclennan, 2018; Neave et al., 2019a). Despite the consensus on variable magma storage depths, conceptual models of the nature and size of the crustal intrusions vary. Some envision an oceanic crust with melt lenses in a pervasive crystal-liquid mush—a mixture of interconnected crystals and magma (Cashman et al., 2017)—whereas others visualize an oceanic crust layered with sills surrounded by solid rock with only trivial crystal-liquid mush on intrusion margins (Maclennan, 2019). In addition, the 'temporal rigidity' of deep magmatic storage is largely unknown. Are the deep roots of volcanoes spatially and temporally fixed, or do the deep portions of the magma transport system reorganize themselves on eruption-to-eruption basis? At least the magmatic systems seem to be flexible in changing their architecture in response to altering surficial loading caused by recurring glaciations (Caracciolo et al., 2019). Shallow silicic magmatic intrusions, typical of evolved central volcanoes, may be long-lived and rigid features in the crust (Flude et al., 2010), whereas magma emplacement in the ductile middle and lower crust may be more indefinite and random.

3 Sampling and laboratory analysis of rocks and minerals

3.1 Samples

For PAPER I, samples containing olivine macrocrysts were gathered from eight locations representing different volcano-tectonic environments in Iceland. From the rift zones (WVZ and NVZ, Fig. 1), I sampled Háleyjabunga lava shield, Mosfellsheiði lava flow field and Kistufell table mountain. From the off-rift volcanic flank zones, I analyzed olivine macrocrysts from Berserkjahraun, Hvammsmúli, Brattaskjól and Stórhöfði lavas and Eyjafjallajökull 2010 tephra (Fig. 1). I separated olivine crystals by handpicking from crushed and sieved (Ø = 0.1–4.0 mm) rock samples, after which they were mounted into epoxy molds or on glass slides. A total of 482 olivine macrocrysts were analyzed for their minor elements (Ni, Mn and Ca specifically) with EPMA, 64 were analyzed for their trace elements with LA-ICP-MS, and analysis of the zoning patterns in olivine was conducted for 34 macrocrysts.

In PAPER II, I further studied the Brattaskjól and Hvammsmúli ankaramite crystal cargo for which the composition of olivine macrocryst cores (n=192) had been determined in PAPER I. Compositions of 51 macrocryst clinopyroxene, 38 spinel and 21 melt inclusions in olivine, and 47 concentration profiles across olivine zonation were measured from thin sections and crystal separates in epoxy molds. As the melt inclusions were partly crystalline in all olivine crystals, they were homogenized by heating to 1200–1220 °C in graphite crucibles prior mounting to epoxy (see Methods in PAPER II).

For the study of the Hafnarhraun lava flow (PAPER III), I initially gathered 54 hand samples, of which 23 were analyzed for whole-rock composition and six thin sections were made for

microchemical examinations and compositional analysis of main minerals (olivine, clinopyroxene and plagioclase). Samples were collected with a steam-hammer developed for taking paleo-magnetic drillcore samples or by rock and chisel, and often by hanging from a rope on the eight-meter-tall quarry wall.

3.2 XRF

X-ray fluorescence (XRF) is the emission of secondary X-rays with characteristic energies and wavelengths, dependent on the atomic structure, when a material is excited with high-energy radiation (X-rays or gamma rays). The compositions of whole-rock samples from the Hafnarhraun pāhoehoe lava lobe (PAPER III) were measured utilizing the XRF phenomenon with a PANalytical Axios mAX 151 4kW WD-XRF spectrometer at the Department of Geosciences and Geography, University of Helsinki. The samples were first crushed using an iron-jawed crusher, wet-sieved with deionized water, and fine-powdered with an agate mill. The rock powders were then mixed in a ratio of 1-part sample powder with 10-parts Li-Borate ultrapure flux (49.5 wt% $Li_2B_4O_7$, 49.5 wt% $LiBO_2$, and 1.0 wt% LiBr) and fused to glass beads using Claisse M4 fluxer. These glass beads were then bombarded with X-rays and the intensity of the X-ray peaks in the secondary X-ray spectra were measured to quantify their major oxide and trace element composition. A total analysis time of 2.5 hours per sample was used to attain an uncertainty of less than <0.05 wt% for all major oxides.

3.3 EPMA

Electron probe microanalyzer (EPMA) is an apparatus for precise non-destructive microanalyses of solid samples. In EPMA, a beam of electrons is produced by an electron source (tungsten filament, Lanthanum Hexaborate crystal cathode, or field emission electron source), accelerated with an anode plate, and directed with electromagnetic condenser lenses to a solid sample. The electron beam interacts with the studied material in various ways, including the production of heat, light (cathodoluminescence), backscattered electrons, secondary electrons, auger electrons, and X-rays. Whereas the electrons and light are useful for imaging purposes, the characteristic X-rays emitted are indicative of the sample composition. To quantify the composition, one can measure the intensity of X-rays of varying energies by energy-dispersive (ED) or wavelength-dispersive (WD) detectors, the difference being that an ED detector counts the intensity of the whole X-ray spectrum at once, while WD detectors can isolate and quantify specific X-ray wavelengths/energies separately.

All EPMA analyses pertinent to this thesis were conducted using a JEOL JXA-8230 electron microprobe at the University of Iceland, equipped with five WD and one silicon drift ED detectors, and a lanthanum hexaborate electron source. For the procedures of major element analyses in olivine, clinopyroxene, plagioclase, spinel and melt inclusions, the reader is referred to the attached papers. Anyhow, the advanced high-precision measurements of minor and trace elements in olivine deserve to be described in some detail here. For these analyses, I used a modified version of a setup of Batanova et al. (2015) and bombarded olivine macrocrysts with unusually high probe-current of 500 nA (compared to 20 nA in standard analyses) and 20 keV acceleration voltage. Analyses were performed with a focused electron beam, and they took 13.25 min per sample spot. Minor and trace elements (Ni, Mn, Ca, Al, Cr, Co, Ti, Zn, P, Na) were measured with WD detectors with peak count times varying from 90 to 150 s, and the EDS was utilized for Si, Mg and Fe measurements with a counting time of 300 s. Grains of San Carlos olivine were measured between every 20–50 analyses

to check for instrumental stability. The setup delivered minor and trace element detection limits of 3–10 ppm, and, crucially, high mean instrumental precisions for Ni (0.52%), Mn (0.48%) and Ca (0.34%). I compared the resulting olivine compositions to earlier analyses of Sobolev et al. (2007), and these were found to be an outstanding match (Electronic Appendix in PAPER I). The success of these olivine minor and trace element analyses was a significant building block for this thesis.

3.4 LA-ICP-MS

For precise trace element analyses of olivine macrocrysts, I utilized laser ablation inductively coupled plasma mass spectrometry (LA-ICP-MS) at the Department of Geosciences and Geography, University of Helsinki. In LA-ICP-MS, a high-intensity laser is used to ablate a small portion (a typical analysis spot diameter of 1-100 μm) of a solid sample, and the produced fine particles are brought to a plasma torch to be ionized and fed to a mass spectrometer. Mass spectrometer is an analytical tool that separates ions based on their mass-to-charge ratio, typically by subjecting them to electromagnetic fields. The amount of deflection in ion paths is mass-to-charge dependent and thus distinct for a specific ion. There are numerous instruments (mass analyzers) to deflect the ions, e.g., the quadrupole mass analyzer utilized in the LA-ICP-MS facility of the University of Helsinki. At the end of the mass spectrometer, the intensity of arriving ions is measured, commonly with an electron multiplier.

I conducted the LA-ICP-MS olivine analyses of PAPER I with the Coherent GeoLas Pro MV 193 nm laser ablation system coupled to an Agilent 7900 s quadrupole ICP–MS at the University of Helsinki. Olivine grains were ablated with a laser spot size of 44 μm and energy density of 7 J/cm^2, and the measurement program included the isotopes: ^{7}Li, ^{23}Na, ^{24}Mg, ^{25}Mg, ^{27}Al, ^{29}Si, ^{43}Ca, ^{31}P, ^{43}Ca, ^{44}Ca, ^{45}Sc, ^{49}Ti, ^{51}V, ^{52}Cr, ^{55}Mn, ^{56}Fe, ^{57}Fe, ^{59}Co, ^{60}Ni, ^{62}Ni, ^{63}Cu, ^{66}Zn, ^{85}Rb, ^{88}Sr and ^{137}Ba. The external standardization was done using GSE 1G synthetic basalt glass, and the Si concentrations determined with high-probe current EPMA analyses were used as internal standards. The data reduction was performed with the SILLS software package (Guillong et al., 2008), and Si-normalized fractionation factors (Fryer et al., 1995) were used to monitor for significant down-hole fractionation or down-hole compositional zonation. The trace element composition of olivine from one location, Háleyjabunga, had been previously analyzed by LA-ICP-MS by Neave et al. (2018). My analyses were found to be slightly higher in Co, but for other elements, the results concurred.

3.5 EBSD

The rate of diffusion in a crystal lattice in olivine is dependent on the crystallographic directions, being nearly three times faster along the olivine c-axis than the a- or b-axes (Dohmen and Chakraborty, 2007; Dohmen et al., 2007). Hence, to use the amount of diffusion in crystal zoning in olivine grains as an indicator of diffusion timescales (PAPER II), the crystallographic orientation of these crystals had to be determined. This was done using electron backscatter diffraction (EBSD, Prior et al., 1999) with FEI Quanta 650 SEM and HKL CHANNEL 5 EBSD software at the University of Leeds. EBSD is a technique of automated analysis of diffraction patterns produced when electrons scatter in a crystal lattice, which can be used to resolve the mineral crystallographic orientation (see Humphreys, 2001).

4 Numerical modelling

4.1 Major, minor and trace elements in olivine as a mantle proxy

Forsterite-rich olivine is typically the first mineral (along with minor spinel) to crystallize from a mantle-derived melt. Therefore, the first-to-crystallize high-Fo olivine is expected to record the composition of its near-primary parental melt before it is masked by crustal magma differentiation. Consequently, high-Fo olivine should store information about the mantle source from which its parental magma was derived (e.g., Sobolev et al., 2007; Herzberg et al., 2016; Matzen et al., 2017b).

Sobolev et al. (2005) were the first to suggest that minor element concentrations in olivine (specifically Ni, Mn and Ca contents) can be used to derive the relative amount of olivine-free pyroxenite in the mantle source of magmas. Since this work, olivine compositions have been used to infer mantle lithology for a wide variety of volcanic settings (e.g., Sobolev et al., 2007; Gurenko et al., 2010; Trela et al., 2015; Herzberg et al., 2016). However, this view of olivine as a proxy of mantle mineralogy has been recently challenged, as new evidence suggests that shifts in partitioning coefficients during mantle melting and subsequent olivine crystallization may in fact be accountable for most, if not all, global variability in olivine compositions (Matzen et al., 2013, 2017a, b; Putirka et al., 2018).

Various mantle rocks produce compositionally diverse mantle melts. For example, partial melts of olivine-free pyroxenites are expected to be richer in Ni than melts of mantle lherzolite, as the abundant olivine in lherzolite effectively sequesters Ni during melting (e.g., Sobolev et al., 2005; Herzberg, 2011). Additionally, the nature of mantle melts varies as a function of the degree and depth of melting. Continuing with Ni as an example, olivine sequesters Ni less effectively at higher T at greater mantle depths (i.e., $D_{Ni}^{ol/liq}$ is lower at higher T, Matzen et al. (2013, 2017a)), and consequently, deep and hot partial melts of lherzolite are higher in Ni compared to lherzolite melts generated at shallower mantle levels. Mildly incompatible elements, for example Sc and Ti that are relevant for olivine studies, are in turn highly susceptible to the degree of mantle melting due to their high incompatibility to mantle minerals (Putirka et al., 2018).

Because influenced by numerous parameters of melting and crystallization, it is challenging to derive a unique explanation for an olivine with a certain minor and trace element composition. High Ni and low Mn in a certain olivine population, for example, may either signal melting of an olivine-poor sources or a deep mantle source region for the magma (see PAPER I). Anyhow, as the knowledge of the partitioning of various elements during mantle melting increases, joint analysis of multiple minor and trace elements (e.g., Ni, Mn, Ca, Sc, Ti, Zn) in olivine may be used to better constrain mantle source characteristics. Furthermore, parameterizations of the temperature- and pressure-dependence of elemental partitioning between olivine and melt can be used to constrain the depth of mantle melting (Matzen et al., 2017b), as attempted in PAPER I.

4.2 Thermodynamic modelling of melting and crystallization

A large part of my thesis revolves around comparing compositional data of rocks and minerals to thermodynamic models of magmatic processes. These models are quantifications of the stability of solid and liquid phases over a range of P and T conditions relevant to igneous systems, rooted to experimentally determined phase stabilities of igneous minerals.

Three thermodynamic modelling programs were used in this thesis: Petrolog3 (Danyush-

evsky and Plechov, 2011), COMAGMAT-5.2.2 (Ariskin et al., 2018), and MELTS (Ghiorso et al., 2002) with ALPHAMELTS 1.8. front end (Smith and Asimow, 2005). Petrolog3 was used to a lesser extent and only to calculate olivine compositions crystallizing from evolving basaltic magmas using the model of Beattie et al. (1993) (e.g., Fig. 8 in PAPER I) and to correct melt inclusion compositions for post-entrapment olivine crystallization and diffusion (see Danyushevsky et al., 2000). The strength of Petrolog3 is that it allows comparison of published mineral-melt equilibrium models (for example, it includes 14 models for olivine-melt equilibrium) and simple calculations can be performed with clearly defined setup. In contrast, the model procedure is fixed in MELTS and COMAGMAT, relying on finding the minimum Gibb's Free Energy (G) of the system under given conditions. MELTS does this directly by testing the stability of phases (whether changes lead to lower G) at a given T using nonlinear mathematical programming (Ghiorso, 1994), whereas COMAGMAT does this indirectly by finding equilibrium for a pre-defined crystallization degree using experimentally determined liquidus temperatures of minerals (Ariskin, 1999; Ariskin et al., 2018). The practical difference between these thermodynamic programs is that MELTS is extremely flexible; it can perform numerous different modelling schemes (to name a few: adiabatic melting, reverse crystallization, near-fractional crystallization) in a large P, T and compositional range. COMAGMAT, in contrast, is calibrated only for basaltic compositions at 1 atm (although usable up to 3 kbar, Ariskin et al. 2018) and tuned for crystallization modelling. Maybe due to this high level of specification, fractional crystallization modelling with COMAGMAT reproduced the compositional trends in the Hafnarhraun lava lobe better than MELTS, and therefore all fractional crystallization modelling was done with the former in PAPER III. MELTS, however, was the only program capable of performing the sophisticated near-fractional adiabatic decompression melting calculations in PAPER I.

4.3 Thermobarometry – probing the crystallization conditions of minerals

The composition of magmatic mineral phases is dependent on the composition of the liquid phase and conditions of crystallization including P, T and fO_2. A prime example of a P-dependent mineral component is jadeite ($NaAlSi_2O_6$; Jd) in clinopyroxene. The stability of Jd increases with increasing pressure, which stems from the significant volume decrease as Jd is produced in the reaction $NaO_{0.5}^{liq} + AlO_{1.5}^{liq} + 2SiO_2^{liq} = NaAlSi_2O_6^{cpx}$, where $NaAlSi_2O_6^{cpx}$ is Jd, and the superscripts denote liquid (liq) and clinopyroxene (cpx). Experimental quantification of this P-sensitive incorporation of Jd in clinopyroxene makes it possible to use measured clinopyroxene-liquid equilibria in volcanic rocks as a barometer, i.e., as a tool to estimate the pressure of crystallization. The most recent formulation of the so-called Jd-in-clinopyroxene barometer (Neave and Putirka, 2017) is as follows (**Equation 1**):

$$\mathrm{P(kbar)} =$$

$$-26.27 + 39.16\frac{\mathrm{T(K)}}{10^4}\ln\left[\frac{\mathrm{X_{Jd}^{Cpx}}}{\mathrm{X_{NaO_{0.5}}^{liq}}\,\mathrm{X_{AlO_{1.5}}^{liq}}\left(\mathrm{X_{SiO_2}^{liq}}\right)^2}\right]$$

$$-4.22\ln\left(X_{DiHd}^{Cpx}\right) + 78.43\mathrm{X_{AlO_{1.5}}^{liq}}$$

$$+393.81\left(\mathrm{X_{NaO_{0.5}}^{liq}}\,\mathrm{X_{KO_{0.5}}^{liq}}\right)^2$$

Here X^{liq} are cation fractions (normalized to 1) and X^{cpx} are clinopyroxene components calculated on the 6 oxygen basis (cation sum close to 4). Jd and DiHd components are calculated using a normative procedure of Putirka et al. (2003). From this formulation, one can see that, in ad-

dition to the compositions of clinopyroxene and host liquid, the barometer is dependent on T. Fortunately, clinopyroxene-liquid equilibrium can also be used as a thermometer, as the partitioning of Diopside-Hedenbergite ($Ca(Mg,Fe)Si_2O_6$; DiHd) and Jd component between clinopyroxene and silicate melt is temperature sensitive (Putirka et al., 1996, 2003). As given in Eq. 33 in Putirka (2008b), the expression of this so-called Jd-DiHd exchange thermometer is (**Equation 2**):

$$\frac{10^4}{T(K)} =$$

$$7.53 - 0.14\ln\left[\frac{X_{\mathrm{Jd}}^{\mathrm{cpx}} X_{CaO}^{liq} X_{Fm}^{liq}}{X_{DiHd}^{\mathrm{cpx}} X_{\mathrm{Na}}^{\mathrm{liq}} X_{Al}^{liq}}\right]$$

$$+0.07(H_2O^{liq}) - 14.9\left(X_{CaO}^{liq} X_{SiO_2}^{liq}\right)$$

$$-0.08\ln\left(X_{TiO_2}^{liq}\right) - 3.62\left(X_{NaO_{0.5}}^{liq} + X_{KO_{0.5}}^{liq}\right)$$

$$-1.1(Mg\#^{liq}) - 0.18ln\left(X_{EnFs}^{cpx}\right) - 0.027P(kbar)$$

Here $X_{\mathrm{Fm}}^{\mathrm{liq}}$ is the Mg+Fe in liquid (cation fractions), H_2O^{liq} is in wt%, and $Mg\#^{\mathrm{liq}}$ is Mg/(Mg+Fe^{2+}) in liquid. Remaining terms are as in Equation 1. Solving Equations 1 and 2 iteratively, using the output of a one model as the input to the other, allows simultaneous estimation of P and T. This, however, requires that the parental melt composition of the studied clinopyroxene crystals is known.

Lava-hosted clinopyroxene macrocrysts are most applicable to thermobarometric studies, as their composition reflects the magmatic storage conditions and subsurface architecture of volcanoes. In these cases, however, the macrocrystic clinopyroxene grains are typically no longer in equilibrium with their carrier lavas, as these lavas tend to have evolved by fractional crystallization and magma mixing after the macrocryst crystallization (Hansen and Grönvold, 2000; Halldorsson et al., 2008; Thomson and Maclennan, 2013). In addition, the macrocryst cargo may have never been in equilibrium with their carrier lavas if the macrocrysts are xenocrysts, i.e., picked by the ascending magmas from unrelated, compositionally distinct magmas or wall rocks. A further problem arises from the presumption of equilibrium crystallization. Numerous experiments have shown that in undercooled magmas, the rapid crystallization of minerals (e.g., clinopyroxene) results in disequilibrium partitioning of elements (e.g., Hammer, 2008; Mollo et al., 2010; Welsch et al., 2016). Furthermore, textural and microchemical evidence indicates that high undercooling and disequilibrium crystallization are common in volcanic magma systems (e.g., Welsch et al., 2016; Ubide et al., 2019).

The challenges related to selecting suitable melts for Jd-in-clinopyroxene thermobarometry require that clinopyroxene-melt equilibrium has to be evaluated using experimentally defined parameters, such as Fe–Mg equilibrium (Wood and Blundy, 1997), minor element contents Ti (e.g., Ti; Hill et al., 2011), and deviation from predicted and measured clinopyroxene componentry (Putirka, 1999; Mollo et al., 2013). In addition, textural inspections of minerals are required to avoid analyzing rapidly crystallized domains that may have disequilibrium compositions (Welsch et al., 2016; Ubide et al., 2019).

In PAPER II, I utilized Jd-in-clinopyroxene thermobarometry to estimate the crystallization pressure and temperature of primitive clinopyroxene crystals in two Eyjafjallajökull ankaramites. As these ankaramites have accumulated macrocrysts (~30% macrocrysts in total), their whole-rock composition does not represent a melt composition, being thus not representative as an equilibrium liquid to be used in thermobarometry. I thus advanced by fitting clinopyroxene compositions to Eyjafjallajökull whole-rock and melt inclusion compositions from Loughin (1995), Moune et al. (2012) and my study, on the basis of chemical equilibrium. First, putative

clinopyroxene-melt pairs were selected with a threshold of ±10 % Fe–Mg equilibrium assuming Kd^{Mg-Fe}(cpx-liq) = 0.27±0.6, for which "pseudo" P and T were calculated. Then, these results were filtered to only include the clinopyroxene-melt pairs that have a measured clinopyroxene composition that concurs with the composition predicted to crystallize from the melt at the given P and T. Specifically, the measured and predicted clinopyroxene compositions had to be in Fe–Mg equilibrium according to Eq. 35 in Putirka (2008b) and agree with respect to CaTs, EnFs and DiHd components within ±0.03 for CaTs (Putirka, 1999), and ±0.05 for EnFs and ±0.06 for DiHd (Mollo et al., 2013). Additionally, the clinopyroxene-liquid pairs had to be within ±40 % of Ti equilibrium (Hill et al., 2011).

Complementary to the Jd-in-clinopyroxene thermobarometry, I used liquid-only (Eq. 15, Putirka, 2008) and olivine-liquid thermometry (Eq. 4, Putirka et al., 2007) for calculating the temperature of olivine crystallization in these ankaramites. I also determined oxygen fugacity during crystallization by comparing compositions of co-crystallized olivine and spinel and using the most recent calibration (Nikolaev et al., 2016) of the Ballhaus-Berry-Green olivine-orthopyroxene-spinel oxybarometer equation (Ballhaus et al., 1991; Beattie, 1993).

4.4 Kinetic modelling of diffusion time scales

Diffusion chronometry (Costa et al., 2008; Zhang and Cherniak, 2010; Dohmen et al., 2017) is a tool for solving magmatic timescales from the amount of diffusion over compositional boundaries in crystals. When being crystallized, a magmatic mineral commonly develops zones of varying composition in response to changes in magma composition and crystallization conditions. While the mineral resides at magmatic temperatures, the initially sharp chemical boundaries diffuse and diminish (Fig. 3a) with a rate typically dependent on T, P, fO_2 and crystallographic orientation. When these are known, the degree of the subsolidus diffusion can be related to the time elapsed between mineral crystallization (e.g., formation of a compositionally distinct rim) and cooling of the crystal. Consequently, the amount of diffusion in minerals can be used to constrain internal dynamics of magma plumbing systems (Kahl et al., 2011, 2015, 2017; Pankhurst et al., 2018), and magma ascent (Rae et al., 2016; Mutch et al., 2019b) and residence times (Mutch et al., 2019a).

In PAPER II, I utilized diffusion chronometry to solve the Fe–Mg diffusion time over compositional boundaries in olivine macrocrysts from Eyjafjallajökull ankaramites. To conduct the iterative calculations of diffusion, I used the Mathematica finite difference diffusion code developed by Maren Kahl (Kahl et al., 2015), and used Fe–Mg inter-diffusion coefficients of Dohmen et al. (2007) and Dohmen and Chakrabortny (2007). Fig. 3b gives an example of the model-fitting for olivine crystal BR02_Ol82 with a so called 'complex reverse zonation', which refers to a core-to-rim zonation pattern where the forsterite content first increases and then sharply decreases in the outer-edge of the crystal. The initial model compositions were set at $Fo_{85.4}$ for the rim and $Fo_{82.4}$ for the core (stippled line). Then, the diffusion model defined the time (9.2 days) of diffusive re-equilibration that is required to produce a zonation pattern (red line) fitting the measured compositional zonation (filled black circles with error bars). The outermost rims in the studied olivine grains have formed, at least partly, by crystallization from cooling and evolving host magma, and not by diffusive re-equilibration only. Therefore, I opted to model the time of diffusive re-equilibration between the olivine core and the high-Fo zone near the crystal edge (Fig. 3b) rather than the re-equilibration between the

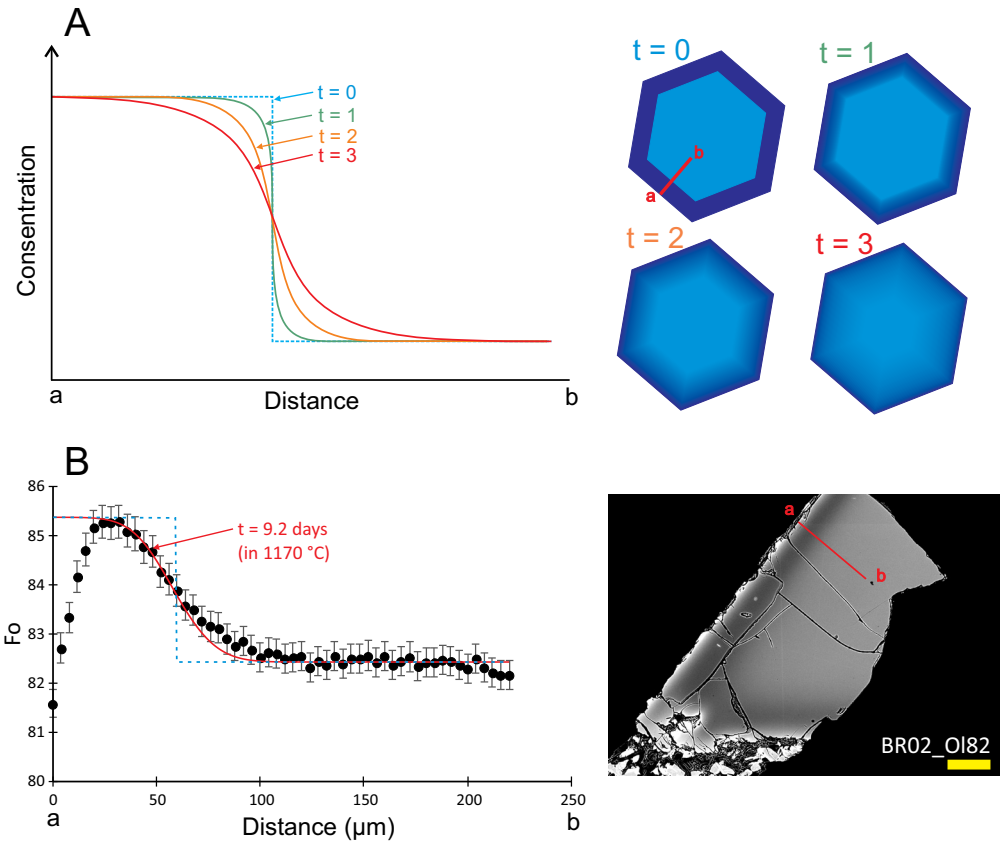

Figure 3. a) Diffusion profile of an element along a traverse a–b in zoned olivine with higher concentration rims (dark blue) and a lower concentration core (light blue). t=0 is the initial state of the system without any diffusive equilibration, t=3 is the last state with the most abundant diffusion. b) An example of diffusion model fitted for an olivine crystal BR02_Ol82. Black dots are the measured forsterite (Fo = 100 × atomic Mg/(Mg + Fe^{2+})) contents in olivine along traverse a–b that is illustrated with a red bar in the BSE image on the right. Error bars correspond to the propagated 2σ error in Fo. The blue stippled line is the model initial state, and the red curve represents the modelled Fo distribution after 9.2 days of diffusive equilibration. The yellow bar is a 100-µm scale bar.

high-Fo zone and the outer crystal rim.

5 Review of original papers

5.1 PAPER I

The compositional variability in basalts erupted in the different volcanic zones of Iceland suggests that the underlying mantle is heterogeneous in composition (Shorttle and Maclennan, 2011; Shorttle et al., 2014). Furthermore, it has been suggested that pyroxenitic mantle domains of recycled oceanic crust contribute to the genesis of Icelandic magmas (Chauvel and Hémond, 2000; Kokfelt et al., 2006). I investigated the mantle source of Iceland basalts by determining the minor and trace element compositions of primitive olivine grains from eight locations around Iceland. As primitive forsteritic olivine is the first mineral to crystallize from most basaltic magmas, it records the composition of its near-primary mantle-derived parental magma and is useful as a mantle proxy. Minor and trace element abundances in olivine, however, do not reflect the mantle source composition only, as they are

dependent on varying olivine-melt distribution coefficients affected by the P–T conditions of melting and subsequent olivine crystallization (Putirka et al., 2018).

Mainly, the new olivine data obtained in this work concur with earlier data, suggesting shallow melting of typical lherzolite mantle as the dominant source of Iceland basalts. However, I also discovered that olivine macrocrysts from the Eyjafjallajökull and Vestmanneyjar volcanic systems in SEVZ are distinctly Mn-poor and Ni-rich compared to olivine from elsewhere in Iceland. Compared to olivine from depleted Iceland rift tholeiite, these SEVZ olivines are also relatively low in Ca, Sc and V and high in Cr, Ti, Zn, Cu and Li. This compositional signature is not easily explained by crustal processes and must be mantle-derived, either indicating the presence of olivine-free mantle domains or high-temperature melting relatively deep in the mantle below the SEVZ.

To examine the cause of the SEVZ olivine signature, I modelled Sc, V, Ti, and Zn partitioning in melting of mantle lherzolite (KLB-1) and pyroxenite-peridotite hybrid (KG2). These numerical models suggest that SEVZ olivine macrocrysts could have been formed by crystallization from low degree lherzolite melts, and only the Zn enrichment may require input from modally enriched mantle domains (e.g., KG2). In the light of these and other results from recent mantle melting models (Lambart, 2017), the SEVZ olivine compositions likely signal high-temperature and high-pressure melting of somewhat enriched olivine-bearing mantle, not an olivine-free mantle source.

The Ni enrichment in the SEVZ olivine macrocrysts suggests melt equilibration depths greater than 45 km, possibly as deep as 66–81 km. Crucial for the survival of this mantle signature in olivine, these deep-derived magmas must have also ascended to the surface relatively fast to avoid re-equilibration and mixing with other mantle derived melts. Seemingly, the off-rift setting at SEVZ favors low-degree melting of deep mantle and swift ascent of these melts, and this is reflected in the olivine compositions in SEVZ basalts.

5.2 PAPER II

To elucidate the conditions of magma storage and differentiation below SEVZ, I analyzed compositions of minerals, mineral zoning patterns, and melt inclusions from the most primitive volcanic rocks identified from Eyjafjallajökull volcanic system: Brattaskjól and Hvammsmúli ankaramites. These ankaramites have ~30 vol% magnesian olivine (up to $Fo_{89.8}$) and clinopyroxene (up to $Mg\#^{cpx}$ 89.8) in near equal proportions and olivine-hosted spinel inclusions that have high $Cr\#^{spl}$ (52–80) and TiO_2 (1–3 wt%) and low Al_2O_3 (8–22 wt%), in comparison with typical Icelandic chromian spinel.

The mineral cargo in these ankaramites is suggestive of mid-crustal crystallization at 10.4±5 km depth over a large temperature interval. Spinel-olivine oxybarometry suggests that olivine-spinel co-crystallization occurred under a moderate oxygen fugacity of ΔlogFMQ 0–0.5. The clinopyroxene-compositions imply crystallization pressures of 1.7–4.2 kbar, averaging at 3.0±1.4 kbar, and crystallization temperatures in the interval 1120–1195 °C. Liquid-only thermometry and olivine-liquid thermometry give somewhat higher crystallization temperatures of 1155–1222 °C and 1136–1213 °C, respectively. Diffusion modelling of the compositional re-equilibration in Brattaskjól olivine macrocrysts suggests that the macrocrysts were mobilized and transported from their crustal storage to the surface within few weeks (within 9–37 days).

Thermobarometric estimations and compositional trends in clinopyroxene suggest that the crystal cargo in Brattaskjól and Hvammsmú-

li ankaramites represents agitated wehrlitic or plagioclase wehrlitic mid-crustal crystal mushes. Evidently, the mid-crustal cotectic assemblage was olivine and clinopyroxene and plagioclase joined the fractionating mineral assemblage later. Compositional trends suggestive of clinopyroxene-dominated crystallization are a known phenomenon in SEVZ lavas, typically regarded as indicative of high (>8 kbar) crystallization pressures (Furman et al., 1991b; Mattsson and Oskarsson, 2005). Our mid-crustal crystallization pressures for Brattaskjól and Hvammsmúli clinopyroxene crystals raise a question whether these high pressures are required to produce clinopyroxene-dominated fractionating assemblages in SEVZ.

5.3 PAPER III

Numerous mechanisms have been suggested that separate crystals and melts from each other in magmatic systems, including gravitational crystal settling (Darwin, 1844), liquid convection (Sparks et al., 1984), filter-pressing (Philpotts et al., 1996), and gas filter-pressing (also called vapor differentiation; Anderson et al., 1984; Sisson and Bacon, 1999; Pistone et al., 2015; Parmigiani et al., 2016). There are two main approaches to the study of these mechanisms: analog experiments and research conducted on solidified differentiated magmatic systems. I took the latter approach and determined the whole-rock and main mineral compositions of a partly differentiated pāhoehoe lava lobe in Hafnarhraun lava flow field, SW Iceland.

The studied 8-m-thick lava lobe (Fig. 4a) includes abundant segregation features: vesicle cylinders (VC) and horizontal vesicle sheets (HVS), commonly interpreted as separated residual melts of the lobe (e.g., Goff, 1996; Caroff et al., 2000; Hartley and Thordarson, 2009). VC are pipe-like, continuous structures up to ~5 cm in diameter that ascend from the base of the lobe and transect the whole lava core (Fig. 4b and d), whereas HVS are vesicular sheets in the upper part of the lava lobe (Fig. 4c), generally a few centimeters thick.

It was found that the whole-rock compositions of VC do not correspond to residual melts generated by fractional crystallization, but rather suggest selective fractionation of plagioclase from the host lava. In addition, the presence of olivine phenocrysts ($Fo_{73–79}$) and microphenocrysts of Ca-plagioclase (An_{77}) in VC indicates that the VC had accumulated primitive crystals in some stage of their evolution. HVS, in turn, were found to occur as two compositional variants in the lava lobe: HVS1 and HVS2. HVS1 are only mildly differentiated in relation to the host lava, commonly include olivine phenocrysts, and are holocrystalline. HVS2, in contrast, correspond to residual melts of the host lava after over 50 % crystallization, and are mineralogically distinct, displaying a texture of flow-aligned plagioclase and having no olivine nor phenocrysts.

Based on the compositional and field evidence, it seems that the VC in the Hafnarhraun lava lobe formed via a two-stage process. First, a combination of residual melt and vapor detached as buoyant diapirs near the lobe base from a mush of olivine, plagioclase, melt and vapor, and later these diapirs accumulated primitive olivine and plagioclase in the lava core. HVS1 represent VC that accumulated at the top of the lava core and spread out as sheets, whereas HVS2 formed independently of VC when residual melts seeped into voids within the upper crust of the lobe. At shallow crustal levels, volatile-aided differentiation processes, such as described from the Hafnarhraun lava lobe, might contribute to the generation of the diversity of basaltic magmas.

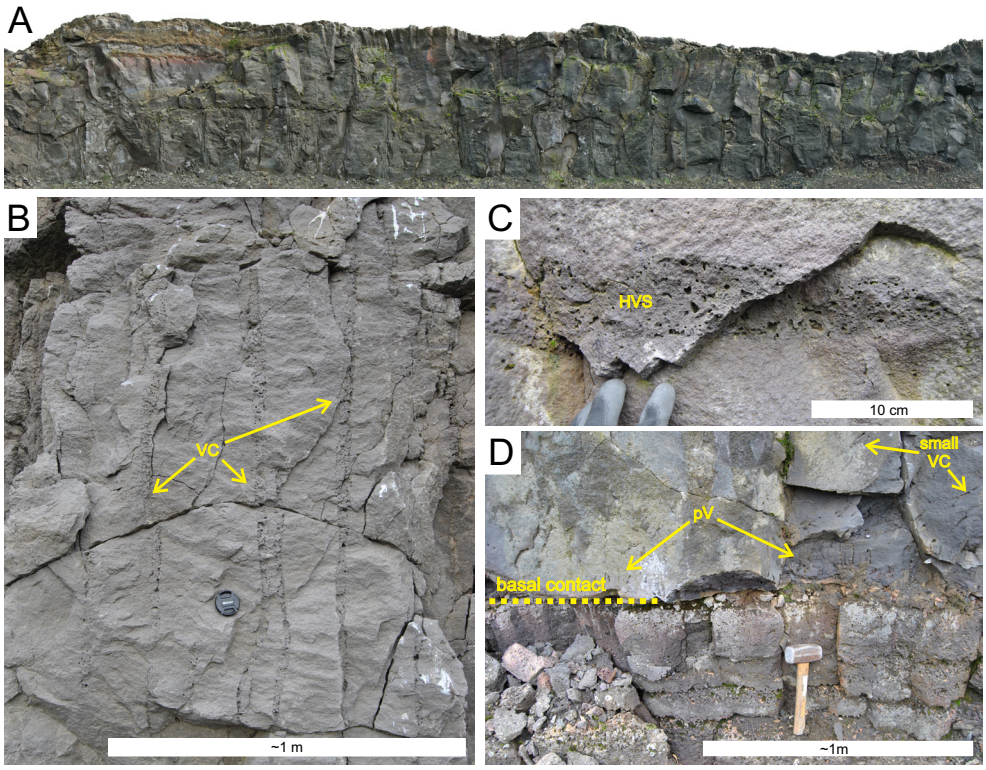

Figure 4. Internal structures of the Hafnarhraun pāhoehoe lobe: a) the studied elongated lava lobe dissected along its crest by a quarry wall, b) vesicle cylinders (VC) in the lava core, c) horizontal vesicle sheet (HVS) in the upper crust d) pipe-vesicles (pV) at the base of the lobe. Photographs by Paavo Nikkola.

6 Discussion

6.1 Dynamics of mantle melting (PAPER I)

The analyses of major, minor and trace elements in olivine macrocrysts from seven Icelandic lavas and one tephra revealed that although most olivine compositions are consistent with a lherzolite mantle as the source of the Iceland basalts, volcanic rocks erupted from Eyjafjallajökull and Vestmannaeyjar in SEVZ carry olivine macrocrysts potentially suggestive of olivine-free, pyroxenitic, mantle source at depth. This is depicted as a kernel density estimation (KDE) in Fig. 5, where I show the compositional parameter of olivine indicating the 'degree of melt derived from olivine-free pyroxenite mantle source' (X_{px}), as parametrized by Gurenko et al. (2010), for Iceland basalts. X_{px} represents the Ni-enrichment and Mn-depletion in olivine at given Fo compared to model-olivines crystallizing from 'canonical' mantle peridotite-derived melts. The Eyjafjallajökull and Vestmannaeyjar olivines show X_{px} values of 0.2–0.7, which are high relative to the X_{px} values of 0–0.4 calculated for olivine grains from the other studied volcanic systems in Iceland.

The X_{px} works well to quantify the difference from olivine expected to crystallize from melts of mantle peridotite, and some have argued for its usefulness as an indicator of the amount of pyroxenite in the mantle source (e.g., Sobolev et al. 2007). However, it is highly doubtful that

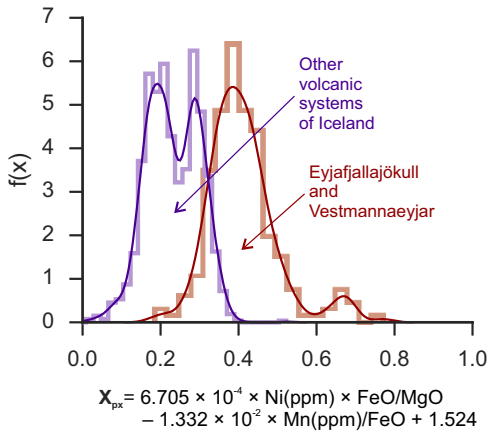

Figure 5. Contribution of melts from pyroxenite mantle to parental magmas (X_{px}) as calculated using the formulation of Gurenko et al. (2010). The curves are kernel density estimates (KDE) fitted with the corresponding histograms of the olivine compositional data. SEVZ olivine data in red and all other Iceland olivine data in violet. Higher X_{px} values can be regarded as representing greater contribution of pyroxenite mantle to aggregated mantle melts (e.g., Sobolev et al., 2007) or higher mantle melting temperatures and greater depth (Matzen et al., 2017b, 2013).

X_{px} has this simple significance, as recent studies demonstrate that higher X_{px} can also reflect an increasing temperature difference between mantle melting and olivine crystallization (Matzen et al., 2017a, b). In addition, mixing between primary and derivate lherzolite magmas can elevate X_{px} (Herzberg et al., 2016). Essentially, in the SEVZ, elevated X_{px} in olivines may simply be attributed to high temperature melting at a great mantle depth caused by the thickened lithosphere in off-rift setting.

Despite the exceptional Ni and Mn contents in SEVZ olivine macrocrysts, other elements in them mainly concur with deep melting of typical olivine-rich lherzolite mantle (KLB-1, Hirose and Kushiro, 1993). I derived this conclusion by modelling the partitioning of Sc, Ti, V and Zn in near-fractional partial melting of a lherzolitic mantle (KLB-1) and then calculating the equilibrium olivine compositions crystallizing from these partial melts, which separate from the mantle at different extents of melting at different depths. In addition, I modelled the composition of olivine crystallizing from partial melts of an olivine-depleted peridotite-pyroxenite hybrid (KG2, Kogiso et al., 1998). The element concentrations of model olivine crystallized from deep-derived, low-degree melts of lherzolite concur with those of the analyzed SEVZ olivine crystals, with the possible exception of Zn, whereas model olivine crystallizing from shallow, high-degree mantle melts are similar to olivine from depleted rift-zone basalt (Háleyjabunga). Even the high Zn in SEVZ olivine grains is not directly indicative of the presence of olivine-free pyroxenite in the mantle source, as an input from KG2 peridotite-pyroxenite hybrid source seems to explain this Zn enrichment.

As nothing in the composition of SEVZ olivine macrocrysts conclusively necessitate olivine-barren pyroxenitic mantle at depth, the deep melting of an olivine-bearing mantle is a more likely candidate in explaining the SEVZ olivine signature. This conclusion is also supported by recent mantle melting models, indicating that relatively silicic melts of olivine-free pyroxenites are prone to react with the surrounding peridotite and hence unlikely to preserve their coherence and compositional signature (Lambart et al., 2012; Lambart, 2017). The high Ni content of the most forsteritic olivine grains suggests a temperature difference between mantle melting and olivine crystallization of 75 ± 3 °C, which, assuming a 55 °C/GPa slope of olivine-saturated liquidus (Sugawara, 2000), translates to a 1.4 GPa pressure difference. Thus, the final mantle equilibration depth of the olivine parental melts must be 45 km or more, if olivine crystallization occurred near the surface, or at depths of 66–81 km, if olivine crystallization occurred in the lower crust (0.6–1.0 GPa pressure). Essentially, I view the SEVZ high-Ni/low-Mn olivine macrocrysts as an indication of the survival of

mantle melts from the deep parts of the mantle melting column, where relatively enriched mantle components like KG2 may reside, to the shallow T–P conditions of olivine crystallization.

Besides SEVZ magmas, deep melting of relatively enriched mantle has been indicated for some rift-zone (Shorttle and Maclennan, 2011) and especially SVZ off-rift magmas (Kokfelt et al., 2006), but there olivine still have MORB-like low-Ni and high-Mn compositions (Herzberg et al., 2016). This is a conundrum: Why the apparent signature of deep mantle melting in olivine from South Iceland magmas in particular? Although I fail to deliver a definitive answer, I suggest that the existence and survival of this signature is due to a favorable crustal and mantle structure below SEVZ. SEVZ is the youngest (activated >3 Ma, Martin et al., 2011) volcanically active zone in Iceland, and hence the underlying mantle may have not yet been depleted in the most fusible domains (e.g., KG2), biasing the melt production to increased depth. In addition, the juvenility of volcanism and low crustal geothermal gradient at SEVZ (Flóvenz and Saemundsson, 1993) is likely reflected in embryonic, small and ephemeral (Sigmarsson, 1996; Mattsson and Oskarsson, 2005) magma storage systems in the crust and upper mantle. These poorly developed magma storage zones favor relatively fast ascent of magmas and allow deep mantle melts to transect the lithosphere with little mixing with mantle melts of shallower origin. This should promote preservation of the deep mantle melting signature in olivine. In contrast, at rift zones and SVZ, magmas derived from different mantle depths and their olivine macrocryst cargo may thoroughly mix and equilibrate in extensive and long-lived crustal magma storage zones, suppressing the potential deep mantle signature in olivine.

This study joins the growing number of other studies expressing skepticism about olivine as a proxy for mantle mineralogy and instead prefer to explain the olivine compositional record as related to the conditions of mantle melting (F, T and P) and subsequent basalt crystallization (Li and Ripley, 2010; Niu et al., 2011; Putirka et al., 2011, 2018; Matzen et al., 2013, 2017b; Heinonen and Fusswinkel, 2017). Nevertheless, major and trace element, as well as isotopic evidence from Iceland lavas suggest the presence of enriched component(s) in the sub-Icelandic mantle (Thirlwall et al., 2004; Shorttle et al., 2014). Moreover, the high-Zn and low-Ca in the analyzed SEVZ olivine grains can be seen suggestive of modally enriched (olivine-poor) mantle source. Therefore, some compositional heterogeneity likely exists in the mantle beneath Iceland.

Recently, Rasmussen et al. (2020) have confirmed the existence of SEVZ olivine signature published in PAPER I, while also presenting a somewhat divergent interpretation regarding the high-Ni and low-Mn in SEVZ olivine macrocrysts. They argue that the SEVZ olivine compositions are, at least partly, indicating pyroxenitic or pyroxenite-peridotite hybrid mantle source, as the lithospheric thickness below SEVZ (~45 km; Árnadóttir et al., 2009; Barnhoorn et al., 2011) is less than the mantle melting depths (up to ~90 km) indicated by NiO/MnO ratios in some of the SEVZ olivine macrocrysts. This argument is reasonable considering the aforementioned notion of the likely existence of enriched mantle components below Iceland; however, it ignores that Icelandic magmas can originate from deeper than the lithosphere-asthenosphere boundary (LAB) and mantle melts do not necessarily equilibrate at LAB before ascending to the lithosphere. Below Iceland, partial melts are sampled from various mantle depths and these melts can keep their compositional coherence at least until mixing and crystallization in crustal intrusions. This is indicated in the trace element and isotopic heterogeneity in melt inclusions (e.g., Maclennan,

2008b, a; Neave et al. 2018) and in geochemical variations in basalts erupted in Iceland rift zones (e.g., Zindler et al., 1979; Shorttle and Maclennan, 2011; Shorttle et al., 2014). SEVZ melts that crystallized the highest Ni and lowest Mn olivine macrocrysts may have been derived deeper than LAB, depths of up to 90 km being still realistic (e.g., Lambart, 2017), and hence elevated NiO/MnO in some olivine macrocrysts at SEVZ does not, by itself, necessitate pyroxenitic mantle source (or any other enriched mantle source) for the region. In addition, the reliability of NiO/MnO in olivine as a mantle indicator, as used in Rasmussen et al. (2020), is hampered in evolved olivine macrocrysts ($Fo_{<88}$), because NiO contents—and thus also NiO/MnO ratios—in olivine crystals are prone to increase in mixing of variably differentiated magmas of a similar mantle source (see Herzberg et al., 2016). Overall, caution is warranted when utilizing NiO and MnO in olivine as an indicator of compositional heterogeneity in the mantle.

For all geochemical mantle proxies (i.e., major and trace element and isotopic composition of magmas), separating the signal of large-scale mantle heterogeneity from that of locally variable conditions of mantle melting is difficult, as the mode of the mantle source and degree and depth of partial melting are expected to be intertwined properties in the production of mantle melts. This dependence is derived from the greater fusibility of modally enriched mantle. Modally enriched mantle domains are only expected to reside in the deep mantle, as partial melting depletes them at a lower pressure. In addition, partial melts of the enriched mantle domains are tapped effectively only at low degrees of partial melting, when they are not diluted by melts of the prevalent depleted mantle. Therefore, if an area—such as SEVZ—erupts magmas suggestive of modally (and isotopically) enriched mantle component at depth, it is not clear whether this component really is (more than usual) abundant below, or if its melts are just tapped effectively by favorable mantle melting (e.g., low melting degree) and transport (e.g. channelized melt flow) conditions. A signal of modally enriched mantle in erupted basalts at a certain area does not necessarily indicate exceptional chemistry in the underlying mantle, as this signal may be due to favorable melting and transport processes, dependent on the physical state of the mantle.

6.2 Magma storage and crystallization in the South Iceland crust (PAPER II)

Analysis of crystals from Eyjafjallajökull ankaramites indicates that at least most of the clinopyroxene and olivine macrocrysts in these rocks have crystallized in mid-crustal pressures (3.0±1.4 kbar), in a large temperature interval (1120–1220 °C), and mostly in absence of plagioclase. In PAPER I, the olivine with high Ni and low Mn contents in these ankaramites did set a minimum mantle equilibration depth of 45 km for the South Iceland magmas. However, if we take 3.0±1.4 kbar as the crystallization pressure of the high-Ni olivine, the final mantle equilibration depth of the olivine host melt is refined to 56±7 km below surface. Furthermore, the high $Cr\#^{spl}$ and TiO_2, and low Al_2O_3 in olivine hosted spinel inclusions identified in PAPER II conform to a deep and enriched mantle source for the olivine host melt suggested by PAPER I.

Fig. 6 depicts the preferred model of crustal ascent and differentiation for Eyjafjallajökull ankaramites. Assuming that the magmatic plumbing system during the formation of Hvammsmúli and Brattaskjól ankaramites resembles the modern volcanic roots of Eyjafjallajökull, multiple lenses of magma reside in the lower crust (A). The degree of solidification of the country rocks at these mid-crustal depths is not certain; however, considering the relatively cold crust at SEVZ

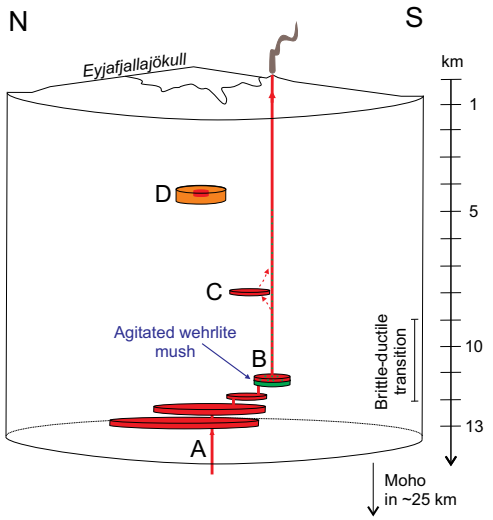

Figure 6. Conceptual model of magma storage below the Eyjafjallajökull volcano. The mantle-derived host magma of the ankaramites ascended and differentiated in mid-crustal magma storage zones (A), agitated a wehrlite crystal-melt mush at 10.7±5 km depth (B), potentially ascended through a shallower intrusion (C), and erupted on the surface. The depth of brittle-ductile transition under Eyjafjallajökull according to Hjaltadóttir et al. (2009). The Eyjafjallajökull 2010 eruption revealed the existence of a benmoreitic magma chamber (D) below the volcano at 5 km depth. It is uncertain whether this evolved magma chamber existed when Hvammsmúli and Brattaskjól ankaramites erupted.

(Flóvenz and Saemundsson, 1993), I envision most of the crust to be below the solidus, and that melt mushes exist only at boundaries of intrusions and near channels of recurring melt transport (see Maclennan, 2019). Somewhere here, a wehrlite mush was agitated and disaggregated to an ascending magma (B). Although all crystallization pressures fall within the 1SEE uncertainty of the Jd-in-clinopyroxene thermometry (±1.4), clinopyroxene with $Mg\#^{cpx}$<83 has the tendency to record lower crystallization pressures. It is thus possible that some clinopyroxene crystallized shallower, maybe in a short-term storage of the magma during magma ascent (C). If the Eyjafjallajökull volcano had a shallow magma chamber (D) during the formation of the Hvammsmúli and Brattaskjól ankaramites, alike it has today, these ankaramite magmas, full of cumulus clinopyroxene and olivine, bypassed it with no interaction.

Identification of mid-crustal formation of a clinopyroxene and olivine-rich mineral assemblage below Eyjafjallajökull is important, in part because clinopyroxene and olivine co-crystallization from SEVZ magmas have been earlier interpreted as indicative of elevated (>8 kbar) magma differentiation pressures (Furman et al., 1991a; Thy, 1991; Mattsson and Oskarsson, 2005). Now, in the light of the new clinopyroxene crystallization pressures, it appears that these lower crustal or upper mantle crystallization conditions are not necessary. This discovery is also timely, as a recent experimental work suggests the co-crystallization of olivine and clinopyroxene from an "enriched end-member" Iceland magma before arrival of plagioclase at the liquidus at only 3 kbar (Neave et al., 2019b). Here, the enriched end-member magma refers to a basaltic magma with high FeO, TiO_2, K_2O and Na_2O contents, and low SiO_2 and CaO contents, compared to depleted end-member basalt in the two-end-member major element classification of Shorttle and Maclennan (2011). SEVZ, where Eyjafjallajökull is located, produce basalts similar to the enriched end-member series (Shorttle and Maclennan, 2011; Shorttle et al., 2014).

If considered in terms of fractional crystallization, the key to stabilizing clinopyroxene before plagioclase in the fractionation assemblage at relatively low pressures is the Ca, Al and H_2O contents in the host magma (Neave et al., 2019b). Addition of water decreases the liquidus temperature of all minerals, but especially plagioclase, suppressing plagioclase crystallization in favor of clinopyroxene and olivine (Gaetani et al., 1993; Feig et al., 2006). Magnesian clinopyroxene could also become stable in intrusive basaltic magma as it evolves while mixing with residual liquids of crystal mushes crystallizing *in situ* near cooling edges of the intrusion (Langmuir, 1989; Hammer et al., 2016). However, yet

there is no need to invoke such a complex model for SEVZ magma genesis, as crystallization experiments with enriched basalts show co-crystallizing olivine and clinopyroxene (Neave et al., 2019b) at 3 kbar. Future research on mush nodules and crustal xenoliths, hosted in many Iceland lavas, should provide deeper insight into how magmatic differentiation really takes place in the Iceland crust.

6.3 Insights to basalt differentiation from the Hafnarhraun lava lobe (PAPER III)

Magmatic differentiation aided by the exsolution of a vapor phase has been invoked to explain differentiated magma lenses and sheets in intrusions (e.g., Carman and Alle, 1994; White, 2007; Zavala et al., 2011), and the formation of crystal-poor Fe-Ti basalts (Sigmarsson et al., 2009) and rhyolites (Parmigiani et al., 2016). In addition, in crustal intrusions, it has been suggested that water vapor can produce density differences in a crystallizing magma body and hence accommodate "bubble-driven convection" (Cardoso and Woods, 1999). The observations from the Hafnarhraun pāhoehoe lobe indicate that vapor exsolution can indeed induce partial convection and compositional variation in solidifying basaltic magma. The effect of vapor on melt circulation was relatively limited, seen as ta sluggish upward movement of segregated material from the solidifying lava base to the upper solidification front, whereas vapor exsolution was efficient in separating residual melts from the bulk crystallizing magma.

In the Hafnarhraun pāhoehoe lobe, vapor-induced differentiation produced two morphological types of vesicular segregation: vesicular cylinders (VC) in the lava core and horizontal vesicle sheets (HVS) in the upper half of the lava lobe. Field evidence and the chemical composition of the segregations suggest that the VC formed as diapirs of residual melt and vapor detached from the lower solidification front of the lava lobe and buoyantly ascended through the lava core. Interestingly, the compositions of VC do not match residual liquids expected to be formed via fractional crystallization of the lobe, as they had accumulated relatively primitive phenocrysts of olivine and microphenocrysts of plagioclase during their ascent in the lava core. HVS, in contrast, developed by two mechanisms, which explains some of the diverging interpretations on the HVS genesis in earlier studies (for example, compare Hartley and Thordarson, 2009; Kuritani et al., 2010). Specifically, HVS can form by accumulation of VC to the upper solidification front of the lobe (mechanism to form HVS1) or when evolved interstitial melts seep into voids in the lava crust (mechanism to form HVS2).

Although volatile exsolution is evidently the culprit in generating chemical heterogeneity within basaltic pāhoehoe lavas, it is uncertain how significant it is for magma differentiation in crustal magmatic systems. Primitive Iceland basalts are expected to be CO_2-saturated but H_2O-undersaturated at mid-crustal (~2–4 kbar) pressures (Lowenstern, 2001), which is their typical pre-ascent storage (Neave and Putirka, 2017; White et al., 2019). Mainly CO_2 (as CO_2-rich fluid) exsolves in response to basalt crystallization at these pressures, and the amount of generated volatiles remains relatively minor. Hence, shallow upper crustal magma storage zones, where H_2O vapor may exist, are more likely environments for volatile-aided differentiation to occur. For example, geophysical anomalies below the Katla volcano are suggestive of a magma chamber at a depth as shallow as 2–3 km (Gudmundsson et al., 1994; Sturkell et al., 2008), and Katla typically produces eruptions of crystal-poor Fe-Ti basalts (Óladóttir et al., 2008). At these low-pressure conditions, and considering the H_2O-en-

riched nature of South Iceland magmas (Moune et al., 2012), differentiation could be aided by exsolution of vapor (Sigmarsson et al., 2009). Furthermore, in more silicic magmas, such as crystal-poor rhyolites, volatile-aided processes of magmatic differentiation are likely important (see Parmigiani et al., 2016) in part due to their higher H_2O content and expansion during volatile saturation (Sisson and Bacon, 1999).

7 Conclusions and future directions

The mantle underneath Iceland must be compositionally heterogeneous. This study, however, did not find evidence of olivine-free domains in the sub-Icelandic mantle. Although an anomalous mantle-source signature in olivine macrocrysts from South Iceland was identified, a closer inspection revealed that these olivines likely crystallized from deep low-degree melts of—potentially somewhat enriched—garnet-peridotite mantle, and an olivine-free mantle source is not necessitated. Future research utilizing isotopic and trace element compositions of South Iceland lavas can build on these findings and better constrain the character of the enriched end-member mantle source below Iceland.

Crystallization of the macrocryst cargo in the Eyjafjallajökull ankaramites Brattaskjól and Hvammsmúli occurred dominantly, if not fully, in the mid-crust (3.0±1.4 kbar; 10.7±5 km). The parental magma (or magmas) had a moderate oxygen fugacity (ΔlogFMQ 0–0.5) and the crystallization occurred over a temperature interval of 1120–1230 °C. The mid-crustal crystallization assemblage was clinopyroxene and olivine, followed by plagioclase, which suggests that elevated lower-crustal pressures (>8 kbar) are not required to produce wehrlitic cumulus assemblages from South Iceland magmas.

At shallow crustal levels, exsolution of volatiles produces density variation in solidifying crystal mushes, which can aid separation of crystals and residual melt. When vapor exsolution occurred within the crystallizing Hafnarhraun pāhoehoe lava lobe, it did not only facilitate separation of residual melt from the bulk crystallizing lava but led to mixing of primitive crystals with these residual melts. As an outcome, magma compositions not predicted by simple models of fractional crystallization were produced. The importance of volatile-aided differentiation in basalt genesis could be elucidated by research on shallow-intrusive bodies aimed to constrain the extent at which vapor exsolution accommodates separation of melts from crystal mushes at various crustal settings.

References

Allègre, J. C., Staudacher, T. and Sarda, P. 1987 Rare gas systematics: formation of the atmosphere, evolution and structure of the Earth's mantle. Earth Planet Sci Lett 81, 127–150. https://doi.org/10.1016/0012-821X(87)90151-8

Anderson, A. T., Swihart, G. H., Artioli, G. and Geiger, C. A. 1984 Segregation vesicles, gas filterpressing, and igneous differentiation. J Geol 92, 55–72. https://doi.org/10.1086/628834

Ariskin, A. A. 1999 Phase equilibria modeling in igneous petrology: use of COMAGMAT model for simulating fractionation of ferro-basaltic magmas and the genesis of high-alumina basalt. J Volcanol Geotherm Res 90, 115–162. https://doi.org/10.1016/S0377-0273(99)00022-0

Ariskin, A. A., Bychkov, K. A., Nikolaev, G. S. and Barmina, G. S. 2018 The COMAGMAT-5: Modeling the effect of Fe-Ni sulfide immiscibility in crystallizing magmas and cumulates. J Petrol 59, 283–298. https://doi.org/10.1093/petrology/egy026

Árnadóttir, T., Lund, B., Jiang, W., et al. 2009 Glacial rebound and plate spreading: Results from the first countrywide GPS observations in Iceland. Geophys J Int 177, 691–716. https://doi.org/10.1111/j.1365-246X.2008.04059.x

Baker, M. B. and Stolper, E. M. 1994 Determining the composition of high-pressure mantle melts using diamond aggregates. Geochim Cosmochim Acta 58, 2811–2827. https://doi.org/10.1016/0016-

7037(94)90116-3
Ballhaus, C., Berry, R. F. and Green, D. H. 1991 High pressure experimental calibration of the olivine-orthopyroxene-spinel oxygen geobarometer: implications for the oxidation state of the upper mantle. Contrib Mineral Petrol 107, 27–40
Barnhoorn, A., van der Wal, W. and Drury, M. R. 2011 Upper mantle viscosity and lithospheric thickness under Iceland. J Geodyn 52, 260–270. https://doi.org/10.1016/j.jog.2011.01.002
Batanova, V. G., Sobolev, A. V. and Kuzmin, D. V. 2015 Trace element analysis of olivine: High precision analytical method for JEOL JXA-8230 electron probe microanalyser. Chem Geol 419, 149–157. https://doi.org/10.1016/j.chemgeo.2015.10.042
Beattie, P. 1993 Olivine-melt and orthopyroxene-melt equilibria. Contrib Mineral Petrol 115, 103–111. https://doi.org/10.1007/BF00712982
Bédard, J. H. 1993 Oceanic crust as a reactive filter: Synkinematic intrusion, hybridization, and assimilation in an ophiolitic magma chamber, western Newfoundland. Geology 21, 77. https://doi.org/10.1130/0091-7613(1993)021<0077:OCAARF>2.3.CO;2
Brounce, M., Feineman, M., LaFemina, P. and Gurenko, A. 2012 Insights into crustal assimilation by Icelandic basalts from boron isotopes in melt inclusions from the 1783-1784 Lakagígar eruption. Geochim Cosmochim Acta 94, 164–180. https://doi.org/10.1016/j.gca.2012.07.002
Brown, E. L. and Lesher, C. E. 2014 North Atlantic magmatism controlled by temperature, mantle composition and buoyancy. Nat Geosci 7, 820–824. https://doi.org/10.1038/ngeo2264
Caracciolo, A., Bali, E., Guðfinnsson, G. H., et al. 2019 Temporal evolution of magma and crystal mush storage conditions in the Bárðarbunga-Veiðivötn volcanic system, Iceland. Lithos. https://doi.org/10.1016/j.lithos.2019.105234
Cardoso, S. S. S. and Woods, A. W. 1999 On convection in a volatile-saturated magma. Earth Planet Sci Lett 168, 301–310. https://doi.org/10.1016/S0012-821X(99)00057-6
Carman, M. F. and Alle. 1994 Mechanisms of differentiation in shallow mafic alkaline instrusions, as illustrated in the Big Bend area, western Texas. J Volcanol Geotherm Res 61, 1–44. https://doi.org/10.1016/0377-0273(94)00008-5
Caroff, M., Maury, R. C., Cotten, J., et al. 2000 Segregation structures in vapor-differentiated basaltic flows. Bull Volcanol 62, 171–187. https://doi.org/10.1007/s004450000077
Cashman, K. V., Sparks, R. S. J. and Blundy, J. D. 2017 Vertically extensive and unstable magmatic systems: A unified view of igneous processes. Science 355, 1–9. https://doi.org/10.1126/science.aag3055
Chauvel, C. and Hémond, C. 2000 Melting of a complete section of recycled oceanic crust: Trace element and Pb isotopic evidence from Iceland. Geochem, Geophys Geosys 1, 1–22. https://doi.org/10.1029/1999GC000002
Clifton, A. E. and Kattenhorn, S. A. 2006 Structural architecture of a highly oblique divergent plate boundary segment. Tectonophysics 419, 27–40. https://doi.org/10.1016/j.tecto.2006.03.016
Costa, F., Dohmen, R. and Chakraborty, S. 2008 Time scales of magmatic processes from modeling the zoning patterns of crystals. Rev Mineral Geochem 69, 545–594. https://doi.org/10.2138/rmg.2008.69.14
Danyushevsky, L. V., Della-Pasqua, F. N. and Sokolov, S. 2000 Re-equilibration of melt inclusions trapped by magnesian olivine phenocrysts from subduction-related magmas: Petrological implications. Contrib Mineral Petrol 138, 68–83. https://doi.org/10.1007/PL00007664
Danyushevsky, L. V. and Plechov, P. 2011 Petrolog3: Integrated software for modeling crystallization processes. Geochem, Geophys Geosys 12. https://doi.org/10.1029/2011GC003516
Darbyshire, F. A., White, R. S. and Priestley, K. F. 2000 Structure of the crust and uppermost mantle of Iceland from a combined seismic and gravity study. Earth Planet Sci Lett 181, 409–428. https://doi.org/10.1016/S0012-821X(00)00206-5
Darwin CR (1844) Geological observations on the volcanic islands visited during the voyages of 519 H.M.S. Beagle, with brief notices on the geology of Australia and the Cape of Good Hope, being the second part of the Voyage of the Beagle. Smith Elder & Co., London.
Davidson, J. P., Morgan, D. J., Charlier, B. L. A., et al. 2007 Microsampling and isotopic analysis of igneous rocks: Implications for the study of magmatic systems. Ann Rev Earth Planet Sci 35, 273–311. https://doi.org/10.1146/annurev.earth.35.031306.140211
Dohmen, R. and Chakraborty, S. 2007 Fe–Mg diffusion in olivine II: point defect chemistry, change of diffusion mechanisms and a model for calculation of diffusion coefficients in natural olivine. Phys Chem Miner 34, 409–430. https://doi.org/10.1007/s00269-007-0158-6
Dohmen, R., Becker, H.-W. and Chakraborty, S. 2007 Fe–Mg diffusion in olivine I: experimental determination between 700 and 1,200°C as a function of composition, crystal orientation and oxygen fugacity. Phys Chem Miner 34, 389–407. https://doi.org/10.1007/s00269-007-0157-7
Dohmen, R., Faak, K. and Blundy, J. D. 2017 Chronometry and speedometry of magmatic processes using chemical diffusion in olivine, plagioclase and pyroxenes. Rev Mineral Geochem. https://doi.org/10.2138/rmg.2017.83.16
Einarsson, P. 2010 Mapping of Holocene surface ruptures in the South Iceland Seismic Zone. Jökull 60, 117–134

Feig, S. T., Koepke, J. and Snow, J. E. 2006 Effect of water on tholeiitic basalt phase equilibria: An experimental study under oxidizing conditions. Contrib Mineral Petrol 152, 611–638. https://doi.org/10.1007/s00410-006-0123-2

Fitton, J., Saunders, A., Norry, M., et al. 1997 Thermal and chemical structure of the Iceland plume. Earth Planet Sci Lett Planet Sci Lett 153, 197–208. https://doi.org/10.1016/S0012-821X(97)00170-2

Flóvenz, Ó. G. and Saemundsson, K. 1993 Heat flow and geothermal processes in Iceland. Tectonophysics 225, 123–138. https://doi.org/10.1016/0040-1951(93)90253-G

Flude, S., McGarvie, D. W., Burgess, R. and Tindle, A. G. 2010 Rhyolites at Kerlingarfjöll, Iceland: The evolution and lifespan of silicic central volcanoes. Bull Volcanol 72, 523–538. https://doi.org/10.1007/s00445-010-0344-0

French, S. W. and Romanowicz, B. 2015 Broad plumes rooted at the base of the Earth's mantle beneath major hotspots. Nature 525, 95–99. https://doi.org/10.1038/nature14876

Fryer, B. J., Jackson, S. E. and Longerich, H. P. 1995 The design, operation and role of the laser-Ablation microprobe coupled with an inductively-coupled plasma - mass-spectrometer (LAM–ICP–MS) in the Earth-Sciences. Can Mineral 33:303–312

Furman, T., Frey, F. A. and Park, K. H. 1991a Chemical constraints on the petrogenesis of mildly alkaline lavas from Vestmannaeyjar, Iceland: the Eldfell (1973) and Surtsey (1963-1967) eruptions. Contrib Mineral Petrol 109, 19–37. https://doi.org/10.1007/BF00687198

Furman, T., Frey, F. A. and Park, K. H. 1991b Chemical constraints on the petrogenesis of mildly alkaline lavas from Vestmannaeyjar, Iceland: the Eldfell (1973) and Surtsey (1963-1967) eruptions. Contrib Mineral Petrol 109, 19–37. https://doi.org/10.1007/BF00687198

Gaetani, G. A., Grove, T. L. and Bryan, W. B. 1993 The influence of water on the petrogenesis of subduction related igneous rocks. Nature 365, 332–334. https://doi.org/10.1038/365332a0

Ghiorso, M. S. 1994 Algorithms for the estimation of phase stability in heterogeneous thermodynamic systems. Geochim Cosmochim Acta 58, 5489–5501. https://doi.org/10.1016/0016-7037(94)90245-3

Ghiorso, M. S., Hirschmann, M. M., Reiners, P. W. and Kress, V. C. 2002 The pMELTS: A revision of MELTS for improved calculation of phase relations and major element partitioning related to partial melting of the mantle to 3 GPa. Geochem, Geophys Geosys 3, 1–35. https://doi.org/10.1029/2001GC000217

Goff, F. 1996 Vesicle cylinders in vapor-differentiated basalt flows. J Volcanol Geotherm Res 71, 167–185. https://doi.org/10.1016/0377-0273(95)00073-9

Green, D. H. and Ringwood, A. E. 1963 Mineral assemblages in a model mantle composition. J Geophys Res 68, 937–945. https://doi.org/10.1029/JZ068i003p00937

Green, D. H. and Ringwood, A. E. 1967 The genesis of basaltic magmas. Contrib Mineral Petrol 15, 103–190. https://doi.org/10.1007/BF00372052

Greenfield, T. and White, R. S. 2015 Building Icelandic igneous crust by repeated melt injections. J Geophys Res Solid Earth 120, 7771–7788. https://doi.org/10.1002/2015JB012009

Gudmundsson, O., Brandsdottir, B., Menke, W. and Sigvaldason, G. E. 1994 The crustal magma chamber of the Katla volcano in south Iceland revealed by 2-D seismic undershooting. Geophys J Int 119, 277–296. https://doi.org/10.1111/j.1365-246X.1994.tb00928.x

Guillong, M., Meier, D. L., Allan, M. M., et al. 2008 SILLS: A matlab-based program for the reduction of laser ablation ICP–MS data of homogeneous materials and inclusions. Mineral Assoc Canada Short Course 40, 328–333

Gurenko, A. A., Hoernle, K. A., Sobolev, A. V., et al. 2010 Source components of the Gran Canaria (Canary Islands) shield stage magmas: evidence from olivine composition and Sr–Nd–Pb isotopes. Contrib Mineral Petrol 159, 689–702. https://doi.org/10.1007/s00410-009-0448-8

Halldorsson, S. A., Oskarsson, N., Gronvold, K., et al. 2008 Isotopic-heterogeneity of the Thjorsa lava-Implications for mantle sources and crustal processes within the Eastern Rift Zone, Iceland. Chem Geol 255, 305–316. https://doi.org/10.1016/j.chemgeo.2008.06.050

Hammer, J. E. 2008 Experimental studies of the kinetics and energetics of magma crystallization. Rev Mineral Geochem 69, 9–59. https://doi.org/10.2138/rmg.2008.69.2

Hammer, J., Jacob, S., Welsch, B., et al. 2016 Clinopyroxene in postshield Haleakala ankaramite: 1. Efficacy of thermobarometry. Contrib Mineral Petrol 171, 1–23. https://doi.org/10.1007/s00410-015-1212-x

Hansen, H. and Grönvold, K. 2000 Plagioclase ultraphyric basalts in Iceland: The mush of the rift. J Volcanol Geotherm Res 98, 1–32. https://doi.org/10.1016/S0377-0273(99)00189-4

Harðardóttir, S., Halldórsson, S. A. and Hilton, D. R. 2018 Spatial distribution of helium isotopes in Icelandic geothermal fluids and volcanic materials with implications for location, upwelling and evolution of the Icelandic mantle plume. Chem Geol 480, 12–27. https://doi.org/10.1016/j.chemgeo.2017.05.012

Hardarson, B. S., Fitton, J. G., Ellam, R. M. and Pringle, M. S. 1997 Rift relocation — A geochemical and geochronological investigation of a palaeo-rift in northwest Iceland. Earth Planet Sci Lett

153, 181–196. https://doi.org/10.1016/S0012-821X(97)00145-3
Hards, V., Kempton, P., Thompson, R. and Greenwood, P. 2000 The magmatic evolution of the Snæfell volcanic centre; an example of volcanism during incipient rifting in Iceland. J Volcanol Geotherm Res 99, 97–121. https://doi.org/10.1016/S0377-0273(00)00160-8
Hart, S. R., Schilling, J. G. and Powell, J. L. 1973 Basalts from Iceland and along the Reykjanes Ridge: Sr isotope geochemistry. Nat Phys Sci 246, 104–107. http://doi.org10.1038/physci246104a0
Hartley, M. and Maclennan, J. 2018 Magmatic densities control erupted volumes in Icelandic volcanic systems. Front Earth Sci 6, 1–9. https://doi.org/10.3389/feart.2018.00029
Hartley, M. E. and Thordarson, T. 2009 Melt segregations in a Columbia River Basalt lava flow: A possible mechanism for the formation of highly evolved mafic magmas. Lithos 112, 434–446. https://doi.org/10.1016/j.lithos.2009.04.003
Heinonen, J. S. and Fusswinkel, T. 2017 High Ni and low Mn/Fe in olivine phenocrysts of the Karoo meimechites do not reflect pyroxenitic mantle sources. Chem Geol 467, 134–142. https://doi.org/10.1016/j.chemgeo.2017.08.002
Hemond, C., Arndt, N. T., Lichtenstein, U., et al. 1993 The heterogeneous Iceland plume: Nd-Sr-O isotopes and trace element constraints. J Geophys Res 98, 15833. https://doi.org/10.1029/93JB01093
Herzberg, C. T. 2004 Partial crystallization of mid-ocean ridge basalts in the crust and mantle. J Petrol 45, 2389–2405. https://doi.org/10.1093/petrology/egh040
Herzberg, C. T. 2011 Identification of source lithology in the Hawaiian and Canary Islands: Implications for origins. J Petrol 52, 113–146. https://doi.org/10.1093/petrology/egq075
Herzberg, C. T. and Asimow, P. D. 2015 PRIMELT3 MEGA.XLSM software for primarymagma calculation: Peridotite primarymagma MgO contents fromthe liquidus to the solidus. Geochem, Geophys Geosys 16, 563–578. https://doi.org/10.1002/2014GC005631
Herzberg, C. T., Vidito, C., Starkey, N. A., et al. 2016 Nickel-cobalt contents of olivine record origins of mantle peridotite and related rocks. Am Mineral 101, 1952–1966. https://doi.org/10.2138/am-2016-5538
Hill, E., Blundy, J. D. and Wood, B. J. 2011 Clinopyroxene-melt trace element partitioning and the development of a predictive model for HFSE and Sc. Contrib Mineral Petrol 161, 423–438. https://doi.org/10.1007/s00410-010-0540-0
Hirose, K. and Kushiro, I. 1993 Partial melting of dry peridotites at high pressures: Determination of compositions of melts segregated from peridotite using aggregates of diamond. Earth Planet Sci Lett 114, 477–489. https://doi.org/10.1016/0012-821X(93)90077-M
Hjaltadóttir, S., Vogfjörð, K. S. and Slunga, R. 2009 Seismic signs of magma pathways through the crust in the Eyjafjallajökull volcano, South Iceland. Icelandic Meteorol Off Rep Vi 2009-013, 1–33
Hofmann, A. W. 1988 Chemical differentiation of the Earth: the relationship between mantle, continental crust, and oceanic crust. Earth Planet Sci Lett. https://doi.org/10.1016/0012-821X(88)90132-X
Hole, M. J. and Natland, J. H. 2019 Magmatism in the North Atlantic Igneous Province; mantle temperatures, rifting and geodynamics. Earth-Sci Rev 1–24. https://doi.org/10.1016/j.earscirev.2019.02.011
Humphreys, F. J. 2001 Grain and subgrain characterisation by electron backscatter diffraction. J Mater Sci 36, 3833–3854. https://doi.org/10.1023/A:1017973432592
Jakobsson, S. P. 1972 Chemistry and distribution pattern of recent basaltic rocks in Iceland. Lithos 5, 365–386. https://doi.org/10.1016/0024-4937(72)90090-4
Jakobsson, S. P., Jónasson, K. and Sigurðsson, I. 2008 The three igneous rock series of Iceland. Jökull 58, 117–138
Jaques, A. L. and Green, D. H. 1980 Anhydrous melting of peridotite at 0-15 Kb pressure and the genesis of tholeiitic basalts. Contrib Mineral Petrol 73, 287–310. https://doi.org/10.1007/BF00381447
Jenkins, J., Cottaar, S., White, R. S. and Deuss, A. 2016 Depressed mantle discontinuities beneath Iceland: Evidence of a garnet controlled 660 km discontinuity? Earth Planet Sci Lett 433, 159–168. https://doi.org/10.1016/j.epsl.2015.10.053
Kahl, M., Chakraborty, S., Costa, F. and Pompilio, M. 2011 Dynamic plumbing system beneath volcanoes revealed by kinetic modeling, and the connection to monitoring data: An example from Mt. Etna. Earth Planet Sci Lett 308, 11–22. https://doi.org/10.1016/j.epsl.2011.05.008
Kahl, M., Chakraborty, S., Pompilio, M. and Costa, F. 2015 Constraints on the nature and evolution of the magma plumbing system of Mt. Etna volcano (1991–2008) from a combined thermodynamic and kinetic modelling of the compositional record of minerals. J Petrol 56, 2025–2068. https://doi.org/10.1093/petrology/egv063
Kahl, M., Viccaro, M., Ubide, T., et al. 2017 A branched magma feeder system during the 1669 eruption of Mt Etna: Evidence from a time-integrated study of zoned olivine phenocryst populations. J Petrol 58, 443–472. https://doi.org/10.1093/petrology/egx022
Kelley, D. F. and Barton, M. 2008 Pressures of crystallization of Icelandic magmas. J Petrol 49, 465–492. https://doi.org/10.1093/petrology/egm089
Kogiso, T., Hirose, K. and Takahashi, E. 1998 Melting experiments on homogeneous mixtures of perido-

tite and basalt: application to the genesis of ocean island basalts. Earth Planet Sci Lett 162, 45–61. https://doi.org/10.1016/S0012-821X(98)00156-3

Kokfelt, T. F., Hoernle, K., Hauff, F., et al. 2006 Combined trace element and Pb-Nd-Sr-O isotope evidence for recycled oceanic crust (upper and lower) in the Iceland mantle plume. J Petrol 47, 1705–1749. https://doi.org/10.1093/petrology/egl025

Kuritani, T., Yoshida, T. and Nagahashi, Y. 2010 Internal differentiation of Kutsugata lava flow from Rishiri Volcano, Japan: Processes and timescales of segregation structures' formation. J Volcanol Geotherm Res 195, 57–68. https://doi.org/10.1016/j.jvolgeores.2010.06.003

Lambart, S. 2017 No direct contribution of recycled crust in Icelandic basalts. Geochemical Perspect Lett 7–12. https://doi.org/10.7185/geochemlet.1728

Lambart, S., Laporte, D., Provost, A. and Schiano, P. 2012 Fate of pyroxenite-derived melts in the peridotitic mantle: Thermodynamic and experimental constraints. J Petrol 53, 451–476. https://doi.org/10.1093/petrology/egr068

Langmuir, C. H., Bender, J. F., Bence, A. E., et al. 1977 Petrogenesis of basalts from the FAMOUS area: Mid-Atlantic Ridge. Earth Planet Sci Lett 36, 133–156. https://doi.org/10.1016/0012-821X(77)90194-7

Langmuir, C. H. 1989 Geochemical consequences of in situ crystallization. Nature 340, 199–205. https://doi.org/10.1038/340199a0

Langmuir, C. and Forsyth, D. 2007 Mantle melting beneath mid-ocean ridges. Oceanography 20, 78–89. https://doi.org/10.5670/oceanog.2007.82

Li, C. and Ripley, E. M. 2010 The relative effects of composition and temperature on olivine-liquid Ni partitioning: Statistical deconvolution and implications for petrologic modeling. Chem Geol 275, 99–104. https://doi.org/10.1016/j.chemgeo.2010.05.001

Loughlin, S. C. 1995 The evolution of the Eyjafjoll volcanic system, southern Iceland. Geology 319

Lowenstern, J. B. 2001 Carbon dioxide in magmas and implications for hydrothermal systems. Mineral Deposita 36, 490–502. https://doi.org/10.1007/s001260100185

Maclennan, J. 2008a Lead isotope variability in olivine-hosted melt inclusions from Iceland. Geochim Cosmochim Acta 72, 4159–4176. https://doi.org/10.1016/j.gca.2008.05.034

Maclennan, J. 2008b Concurrent mixing and cooling of melts under Iceland. J Petrol 49, 1931–1953. https://doi.org/10.1093/petrology/egn052

Maclennan, J. 2019 Mafic tiers and transient mushes: Evidence from Iceland. Philos Trans R Soc A Math Phys Eng Sci 377, 1–20. https://doi.org/10.1098/rsta.2018.0021

Maclennan, J., Mckenzie, D. and Gronvold, K. 2001a Plume-driven upwelling under Central Iceland. Earth Planet Sci Lett 194, 67–82. https://doi.org/10.1016/S0012-821X(01)00553-2

Maclennan, J., McKenzie, D., Gronvöld, K. and Slater, L. 2001b Crustal accretion under Northern Iceland. Earth Planet Sci Lett 191, 295–310. https://doi.org/10.1016/S0012-821X(01)00420-4

Martin, E., Paquette, J. L., Bosse, V., et al. 2011 Geodynamics of rift-plume interaction in Iceland as constrained by new $^{40}Ar/^{39}Ar$ and in situ U-Pb zircon ages. Earth Planet Sci Lett 311, 28–38. https://doi.org/10.1016/j.epsl.2011.08.036

Mattsson, H. B. and Oskarsson, N. 2005 Petrogenesis of alkaline basalts at the tip of a propagating rift: Evidence from the Heimaey volcanic centre, south Iceland. J Volcanol Geotherm Res 147, 245–267. https://doi.org/10.1016/j.jvolgeores.2005.04.004

Matzen, A. K., Baker, M. B., Beckett, J. R. and Stolper, E. M. 2013 The temperature and pressure dependence of nickel partitioning between olivine and silicate melt. J Petrol 54, 2521–2545. https://doi.org/10.1093/petrology/egt055

Matzen, A. K., Baker, M. B., Beckett, J. R., et al. 2017a The effect of liquid composition on the partitioning of Ni between olivine and silicate melt. Contrib Mineral Petrol 172, 3. https://doi.org/10.1007/s00410-016-1319-8

Matzen, A. K., Wood, B. J., Baker, M. B. and Stolper, E. M. 2017b The roles of pyroxenite and peridotite in the mantle sources of oceanic basalts. Nat Geosci 10, 530–535. https://doi.org/10.1038/ngeo2968

McDonough, W. F. and Sun, S. s. 1995 The composition of the Earth. Chem Geol 120, 223–253. https://doi.org/10.1016/0009-2541(94)00140-4

Mckenzie, D. and O'nions, R. K. 1991 Partial melt distributions from inversion of rare earth element concentrations. J Petrol. https://doi.org/10.1093/petrology/32.5.1021

Mollo, S., Del Gaudio, P., Ventura, G., et al. 2010 Dependence of clinopyroxene composition on cooling rate in basaltic magmas: Implications for thermobarometry. Lithos 118, 302–312. https://doi.org/10.1016/j.lithos.2010.05.006

Mollo, S., Putirka, K., Misiti, V., et al. 2013 A new test for equilibrium based on clinopyroxene-melt pairs: Clues on the solidification temperatures of Etnean alkaline melts at post-eruptive conditions. Chem Geol 352, 92–100. https://doi.org/10.1016/j.chemgeo.2013.05.026

Moorbath, S., Sigurdsson, H. and Goodwin, R. 1968 K–Ar ages of the oldest exposed rocks in Iceland. Earth Planet Sci Lett 4, 197–205. https://doi.org/10.1016/0012-821X(68)90035-6

Moune, S., Sigmarsson, O., Schiano, P., et al. 2012 Melt inclusion constraints on the magma source of Eyjafjallajökull 2010 flank eruption. J Geophys Res Solid Earth 117, 1–13. https://doi.org/10.1029/2011JB008718

Mutch, E. J. F., Maclennan, J., Holland, T. J. B. and

Buisman, I. 2019a Millennial storage of near-Moho magma. Science 365, 260–264. https://doi.org/10.1126/science.aax4092

Mutch, E. J. F., Maclennan, J., Shorttle, O., et al. 2019b Rapid transcrustal magma movement under Iceland. Nat Geosci 12, 569–574. https://doi.org/10.1038/s41561-019-0376-9

Neave, D. A., Passmore, E., Maclennan, J., et al. 2013 Crystal-melt relationships and the record of deep mixing and crystallization in the ad 1783 laki eruption, Iceland. J Petrol 54, 1661–1690. https://doi.org/10.1093/petrology/egt027

Neave, D. A., Maclennan, J., Hartley, M. E., et al. 2014 Crystal storage and transfer in basaltic systems: The Skuggafjöll eruption, Iceland. J Petrol 55, 2311–2346. https://doi.org/10.1093/petrology/egu058

Neave, D. A. and Putirka, K. D. 2017 A new clinopyroxene-liquid barometer, and implications for magma storage pressures under Icelandic rift zones. Am Mineral 102, 777–794. https://doi.org/10.2138/am-2017-5968

Neave, D. A., Shorttle, O., Oeser, M., et al. 2018 Mantle-derived trace element variability in olivines and their melt inclusions. Earth Planet Sci Lett 483, 90–104. https://doi.org/10.1016/j.epsl.2017.12.014

Neave, D. A., Bali, E., Guðfinnsson, G. H., et al. 2019a Clinopyroxene–liquid equilibria and geothermobarometry in natural and experimental tholeiites: the 2014–2015 Holuhraun eruption, Iceland. J Petrol. https://doi.org/10.1093/petrology/egz042

Neave, D. A., Namur, O., Shorttle, O. and Holtz, F. 2019b Magmatic evolution biases basaltic records of mantle chemistry towards melts from recycled sources. Earth Planet Sci Lett 520, 199–211. https://doi.org/10.1016/j.epsl.2019.06.003

Nikolaev, G. S., Ariskin, A. A., Barmina, G. S., et al. 2016 Test of the Ballhaus–Berry–Green Ol–Opx–Sp oxybarometer and calibration of a new equation for estimating the redox state of melts saturated with olivine and spinel. Geochemistry Int 54, 301–320. https://doi.org/10.1134/S0016702916040078

Niu, Y., Wilson, M., Humphreys, E. R. and O'Hara, M. J. 2011 The origin of intra-plate ocean island basalts (OIB): The lid effect and its geodynamic implications. J Petrol 52, 1443–1468. https://doi.org/10.1093/petrology/egr030

O'Hara, M. J. 1968 The bearing of phase equilibria studies in synthetic and natural systems on the origin and evolution of basic and ultrabasic rocks. Earth-Sci Rev 4, 69–133. https://doi.org/10.1016/0012-8252(68)90147-5

Óladóttir, B. A., Sigmarsson, O., Larsen, G. and Thordarson, T. 2008 Katla volcano, Iceland: Magma composition, dynamics and eruption frequency as recorded by Holocene tephra layers. Bull Volcanol 70, 475–493. https://doi.org/10.1007/s00445-007-0150-5

Oskarsson, N., Sigvaldason, G. E. and Steinthórsson, S. 1982 A dynamic model of rift zone petrogenesis and the regional petrology of Iceland. J Petrol 23, 28–74. https://doi.org/10.1093/petrology/23.1.28

Oskarsson, N., Steinthorsson, S. and Sigvaldason, G. E. 1985 Iceland geochemical anomaly: Origin, volcanotectonics, chemical fractionation and isotope evolution of the crust. J Geophys Res 90, 10011. https://doi.org/10.1029/JB090iB12p10011

Pankhurst, M. J., Morgan, D. J., Thordarson, T. and Loughlin, S. C. 2018 Magmatic crystal records in time, space, and process, causatively linked with volcanic unrest. Earth Planet Sci Lett 493, 231–241. https://doi.org/10.1016/j.epsl.2018.04.025

Parmigiani, A., Faroughi, S., Huber, C., et al. 2016 Bubble accumulation and its role in the evolution of magma reservoirs in the upper crust. Nature 532, 492–495. https://doi.org/10.1038/nature17401

Philpotts, A. R., Carroll, M. and Hill, J. M. 1996 Crystal-mush compaction and the origin of pegmatitic segregation sheets in a thick flood-basalt flow in the Mesozoic Hartford Basin, Connecticut. J Petrol 37, 811–836. https://doi.org/10.1093/petrology/37.4.811

Pistone, M., Arzilli, F., Dobson, K. J., et al. 2015 Gas-driven filter pressing in magmas: Insights into in-situ melt segregation from crystal mushes. Geology 43, 699–702. https://doi.org/10.1130/G36766.1

Presnall, D. C. and Gudfinnsson, G. H. 2011 Oceanic volcanism from the low-velocity zone - without mantle plumes. J Petrol 52, 1533–1546. https://doi.org/10.1093/petrology/egq093

Presnall, D. C., Dixon, S. A., Dixon, J. R., et al. 1978 Liquidus phase relations on the join diopside-forsterite-anorthite from 1 atm to 20 kbar: Their bearing on the generation and crystallization of basaltic magma. Contrib Mineral Petrol 66, 203–220. https://doi.org/10.1007/BF00372159

Presnall, D. C., Gudfinnsson, G. H. and Walter, M. J. 2002 Generation of mid-ocean ridge basalts at pressures from 1 to 7 GPa. Geochim Cosmochim Acta 66, 2073–2090. https://doi.org/10.1016/S0016-7037(02)00890-6

Prior, D. J., Boyle, A. P., Brenker, F., et al. 1999 The application of electron backscatter diffraction and orientation contrast imaging in the SEM to textural problems in rocks. Am Mineral 84, 1741–1759. https://doi.org/10.2138/am-1999-11-1204

Putirka, K. 1999 Clinopyroxene + liquid equilibria to 100 kbar and 2450 K. Contrib Mineral Petrol 135, 151–163. https://doi.org/10.1007/s004100050503

Putirka, K. 2008a Excess temperatures at ocean islands: Implications for mantle layering and convection. Geology 36, 283. https://doi.org/10.1130/G24615A.1

Putirka, K. D. 2008b Thermometers and barometers

for volcanic systems. Rev Mineral Geochem 69, 61–120. https://doi.org/10.2138/rmg.2008.69.3

Putirka, K. 2016 Rates and styles of planetary cooling on Earth, Moon, Mars, and Vesta, using new models for oxygen fugacity, ferric-ferrous ratios, olivine-liquid Fe-Mg exchange, and mantle potential temperature. Am Mineral 101, 819–840. https://doi.org/10.2138/am-2016-5402

Putirka, K., Johnson, M., Kinzler, R., et al. 1996 Thermobarometry of mafic igneous rocks based on clinopyroxene-liquid equilibria, 0-30 kbar. Contrib Mineral Petrol 123, 92–108. https://doi.org/10.1007/s004100050145

Putirka, K., Ryerson, F. J., Perfit, M. and Ridley, W. I. 2011 Mineralogy and composition of the oceanic mantle. J Petrol 52, 279–313. https://doi.org/10.1093/petrology/egq080

Putirka, K. D., Mikaelian, H., Ryerson, F. and Shaw, H. 2003 New clinopyroxene-liquid thermobarometers for mafic, evolved, and volatile-bearing lava compositions, with applications to lavas from Tibet and the Snake River Plain, Idaho. Am Mineral 88, 1542–1554. https://doi.org/10.2138/am-2003-1017

Putirka, K. D., Perfit, M., Ryerson, F. J. and Jackson, M. G. 2007 Ambient and excess mantle temperatures, olivine thermometry, and active vs. passive upwelling. Chem Geol 241, 177–206. https://doi.org/10.1016/j.chemgeo.2007.01.014

Putirka, K., Tao, Y., Hari, K. R. R., et al. 2018 The mantle source of thermal plumes: Trace and minor elements in olivine and major oxides of primitive liquids (and why the olivine compositions don't matter). Am Mineral 103, 1253–1270. https://doi.org/10.2138/am-2018-6192

Rae, A. S. P., Edmonds, M., Maclennan, J., et al. 2016 Time scales of magma transport and mixing at Kīlauea Volcano, Hawai'i. Geology 44, 463–466. https://doi.org/10.1130/G37800.1

Rasmussen, M. B., Halldórsson, S. A., Gibson, S. A. and Guðfinnsson, G. H. 2020 Olivine chemistry reveals compositional source heterogeneities within a tilted mantle plume beneath Iceland. Earth Planet Sci Lett 531, 116008. https://doi.org/10.1016/j.epsl.2019.116008

Schilling, J. G. 1973 Iceland mantle plume: Geochemical study of Reykjanes Ridge. Nature 242, 565–571. https://doi.org/10.1038/242565a0

Shorttle, O. and Maclennan, J. 2011 Compositional trends of Icelandic basalts: Implications for short-length scale lithological heterogeneity in mantle plumes. Geochem, Geophys Geosys 12. https://doi.org/10.1029/2011GC003748

Shorttle, O., Maclennan, J. and Lambart, S. 2014 Quantifying lithological variability in the mantle. Earth Planet Sci Lett 395, 24–40. https://doi.org/10.1016/j.epsl.2014.03.040

Sigmarsson, O. 1996 Short magma chamber residence time at an Icelandic volcano inferred from U-series disequilibria. Nature 382, 440–442. https://doi.org/10.1038/382440a0

Sigmarsson, O. and Steinthórsson, S. 2007 Origin of Icelandic basalts: A review of their petrology and geochemistry. J Geodyn 43, 87–100. https://doi.org/10.1016/j.jog.2006.09.016

Sigmarsson, O., Thordarson, T. and Jakobsson, S. P. 2009 Segregations in Surtsey lavas (Iceland) reveal extreme magma differentiation during late stage flow emplacement. Spec Publ IAVCEI 85–104. https://doi.org/10.1182/blood-2015-09-672774

Sigmundsson, F., Einarsson, P., Rut, Á., et al. 2018 Geodynamics of Iceland and the signatures of plate spreading. J Volcanol Geotherm Res. https://doi.org/10.1016/j.jvolgeores.2018.08.014

Sisson, T. W. and Bacon, C. R. 1999 Gas-driven filter pressing in magmas. Geology 27, 613–616. https://doi.org/10.1130/0091-7613(1999)027<0613:GDFPIM>2.3.CO

Smith, P. M. and Asimow, P. D. 2005 Adiabat-1ph: A new public front-end to the MELTS, pMELTS, and pHMELTS models. Geochem, Geophys Geosys 6, 1–8. https://doi.org/10.1029/2004GC000816

Sobolev, A. V., Hofmann, A. W., Sobolev, S. V. and Nikogosian, I. K. 2005 An olivine-free mantle source of Hawaiian shield basalts. Nature 434, 590–597. https://doi.org/10.1038/nature03411

Sobolev, A. V., Hofmann, A. W., Kuzmin, D. V., et al. 2007 The amount of recycled crust in sources of mantle-derived melts. Science 316, 412–7. https://doi.org/10.1126/science. 1138113

Sollas,W. J. (1894). On the volcanic district of Carlingford and Slieve Gullion. Part I: On the relation of the granite to the gabbro of Barnavave, Carlingford. Transactions of the Royal Irish Academy 30: 477–512.

Sparks, R. S. J., Huppert, H. E., Turner, J. S., et al. 1984 The fluid dynamics of evolving magma chambers. Philos Trans R Soc Lond 310, 511–534. https://doi.org/10.1098/rsta.1984.0006

Stefansson, R., Gudmundsson, G. B. and Halldorsson, P. 2008 Tjörnes fracture zone. New and old seismic evidences for the link between the North Iceland rift zone and the Mid-Atlantic ridge. Tectonophysics 447, 117–126. https://doi.org/10.1016/j.tecto.2006.09.019

Steinthorsson, S., Oskarsson, N. and Sigvaldason, G. E. 1985 Origin of alkali basalts in Iceland: A plate tectonic model. J Geophys Res 90, 10027. https://doi.org/10.1029/JB090iB12p10027

Stolper, E. 1980 A phase diagram for mid-ocean ridge basalts: Preliminary results and implications for petrogenesis. Contrib Mineral Petrol 74, 13–27. https://doi.org/10.1007/BF00375485

Sturkell, E., Einarsson, P., Roberts, M. J., et al. 2008 Seismic and geodetic insights into magma accumulation at Katla subglacial volcano, Iceland: 1999 to 2005. J Geophys Res Solid Earth 113, 1–17. https://doi.org/10.1029/2006JB004851

Sugawara, T. 2000 Empirical relationships between temperature, pressure, and MgO content in olivine and pyroxene saturated liquid. J Geophys Res 105, 8457. https://doi.org/10.1029/2000JB900010

Sun, S.-S. and Jahn, B. 1975 Lead and strontium isotopes in post-glacial basalts from Iceland. Nature 255, 527–530. https://doi.org/10.1038/255527a0

Tarasewicz, J., Brandsdóttir, B., White, R. S., et al. 2012 Using microearthquakes to track repeated magma intrusions beneath the Eyjafjallajökull stratovolcano, Iceland. J Geophys Res Solid Earth 117, 1–13. https://doi.org/10.1029/2011JB008751

Thirlwall, M. F., Gee, M. A. M., Taylor, R. N. and Murton, B. J. 2004 Mantle components in Iceland and adjacent ridges investigated using double-spike Pb isotope ratios. Geochim Cosmochim Acta 68, 361–386. https://doi.org/10.1016/S0016-7037(03)00424-1

Thomson, A. and Maclennan, J. 2013 The distribution of olivine compositions in Icelandic basalts and picrites. J Petrol 54, 745–768. https://doi.org/10.1093/petrology/egs083

Thordarson, T. and Larsen, G. 2007 Volcanism in Iceland in historical time: Volcano types, eruption styles and eruptive history. J Geodyn 43, 118–152. https://doi.org/10.1016/j.jog.2006.09.005

Thy, P. 1991 High and low pressure phase equilibria of a mildly alkalic lava from the 1965 Surtsey eruption: Experimental results. Lithos 26, 223–243. https://doi.org/10.1016/0024-4937(91)90030-O

Trela, J., Vidito, C., Gazel, E., et al. 2015 Recycled crust in the galápagos plume source at 70 ma: Implications for plume evolution. Earth Planet Sci Lett 425, 268–277. https://doi.org/10.1016/j.epsl.2015.05.036

Ubide, T., Mollo, S., Zhao, J., et al. 2019 Sector-zoned clinopyroxene as a recorder of magma history, eruption triggers, and ascent rates. Geochim Cosmochim Acta 251, 265–283. https://doi.org/10.1016/j.gca.2019.02.021

Welsch, B., Hammer, J., Baronnet, A., et al. 2016 Clinopyroxene in postshield Haleakala ankaramite: 2. Texture, compositional zoning and supersaturation in the magma. Contrib Mineral Petrol 171, 1–19. https://doi.org/10.1007/s00410-015-1213-9

White, C. M. 2007 The graveyard point intrusion: An example of extreme differentiation of snake river plain basalt in a shallow crustal pluton. J Petrol 48, 303–325. https://doi.org/10.1093/petrology/egl062

White, R. and McKenzie, D. 1989 Magmatism at rift zones: The generation of volcanic continental margins and flood basalts. J Geophys Res 94, 7685. https://doi.org/10.1029/JB094iB06p07685

White, R. S., Edmonds, M., Maclennan, J., et al. 2019 Melt movement through the Icelandic crust. Philos Trans R Soc A Math Phys Eng Sci 377, 1–22. https://doi.org/10.1098/rsta.2018.0010

Wilson, J. T. 1963 Evidence from islands on the spreading of ocean floors. Nature 197, 536–538

Wolfe, C. J., Bjarnason, I. T., VanDecar, J. C. and Solomon, S. C. 1997 Seismic structure of the Iceland mantle plume. Nature 385, 245–247. https://doi.org/10.1038/385245a0

Wood, B. J. and Blundy, J. D. 1997 A predictive model for rare earth element partitioning between clinopyroxene and anhydrous silicate melt. Contrib Mineral Petrol 129, 166–181. https://doi.org/10.1007/s004100050330

Zavala, K., Leitch, A. M. and Fisher, G. W. 2011 Silicic segregations of the Ferrar Dolerite sills, Antarctica. J Petrol 52, 1927–1964. https://doi.org/10.1093/petrology/egr035

Zhang, Y. and Cherniak, D. 2010 Diffusion in Minerals and Melts. Rev Mineral Geochem. https://doi.org/10.2138/rmg.2010.72.2

Zindler, A., Hart, S. R., Frey, F. A. and Jakobsson, S. P. 1979 Nd and Sr isotope ratios and rare earth element abundances in Reykjanes Peninsula basalts evidence for mantle heterogeneity beneath Iceland. Earth Planet Sci Lett 45, 249–262. https://doi.org/10.1016/0012-821X(79)90127-4

Appendix I. Compositions of clinopyroxene of Brattaskjól ankaramite (data related to Paper II)

Brattaskjól

Analysis[1]	Anal. Loc[2]	Mg#^{cpx}	SiO_2	TiO_2	Al_2O_3	FeO	MnO	MgO	CaO	Na2O	Cr_2O_3	NiO	Total
BR02cpx_cp1_AVG	CORE	84.7	50.96	0.80	4.26	5.25	0.10	16.31	21.29	0.25	0.06	0.01	99.28
BR02cpx_cp2_AVG	CORE	85.7	51.68	0.72	3.57	4.99	0.10	16.73	21.14	0.24	0.39	0.04	99.60
BR02cpx_cp3_AVG	CORE	84.2	50.96	0.76	4.50	5.36	0.10	16.06	21.36	0.25	0.35	0.02	99.71
BR02cpx_cp4_AVG	CORE	83.3	50.40	0.97	4.50	5.61	0.11	15.73	21.48	0.26	0.49	0.02	99.59
BR02cpx_cp5_AVG	CORE	84.3	51.32	0.75	4.00	5.39	0.11	16.23	21.26	0.26	0.45	0.03	99.79
BR02cpx_cp6_AVG	CORE	86.0	51.26	0.62	3.62	4.84	0.11	16.67	21.16	0.27	0.75	0.03	99.33
BR02cpx_cp7_AVG	CORE	84.8	50.60	0.85	4.16	5.12	0.11	16.03	21.43	0.29	0.68	0.04	99.32
BR02cpx_cp8_AVG	CORE	82.4	50.42	1.01	4.00	5.98	0.11	15.71	21.18	0.26	0.46	0.03	99.16
BR02cpx_cp9_AVG	CORE	85.1	50.99	0.76	4.13	5.08	0.11	16.34	21.29	0.25	0.64	0.03	99.62
BR02cpx_cp10_AVG	CORE	80.8	50.30	1.09	3.91	6.58	0.14	15.58	21.22	0.28	0.16	0.03	99.29
BR02cpx_cp11_AVG	CORE	86.7	51.08	0.59	3.68	4.58	0.09	16.70	20.88	0.27	1.23	0.03	99.13
BR02cpx_cp13_AVG	CORE	80.4	51.11	1.04	3.42	6.81	0.13	15.72	21.34	0.26	0.08	0.01	99.91
BR02cpx_cp14_AVG	CORE	89.8	53.04	0.36	2.25	3.68	0.10	18.11	20.63	0.27	1.10	0.04	99.59
BR02cpx_cp15_AVG	CORE	89.8	53.05	0.38	2.19	3.68	0.09	18.17	20.47	0.26	1.12	0.03	99.43
BR02cpx_cp16_AVG	CORE	83.9	51.29	0.62	3.49	5.64	0.12	16.46	20.98	0.26	0.44	0.02	99.31
BR02cpx_cp17_AVG	CORE	83.6	50.92	0.86	4.20	5.60	0.11	16.01	21.56	0.27	0.13	0.02	99.68
BR02cpx_cp18_AVG	CORE	89.7	53.18	0.36	2.22	3.71	0.09	18.17	20.76	0.28	1.09	0.05	99.92
BR02cpx_cp19_AVG	CORE	82.4	50.96	0.92	3.63	6.09	0.12	16.01	21.13	0.26	0.35	0.01	99.48
BR02cpx_cp20_AVG	CORE	82.5	50.57	1.00	3.90	5.98	0.12	15.82	21.61	0.25	0.38	0.02	99.64
BR02cpx_cp21_AVG	CORE	85.5	51.15	0.73	4.00	4.97	0.10	16.43	21.29	0.27	0.76	0.04	99.74
BR02cpx_cp22_AVG	CORE	81.7	50.81	1.02	3.75	6.26	0.13	15.68	21.45	0.28	0.19	0.03	99.59
BR02cpx_cp23_AVG	CORE	86.4	51.57	0.64	3.63	4.67	0.09	16.63	21.18	0.28	0.87	0.03	99.59
BR02cpx_cp24_AVG	CORE	86.7	52.26	0.57	3.15	4.68	0.10	17.18	20.82	0.28	0.68	0.02	99.76
BR02cpx_cp25_AVG	CORE	83.1	50.84	1.04	3.95	5.71	0.11	15.72	21.57	0.25	0.46	0.01	99.67
BR02cpx_cp26_AVG	CORE	86.9	52.14	0.52	2.97	4.62	0.10	17.21	20.97	0.27	0.87	0.03	99.70
BR02cpx_cp27_AVG	CORE	83.2	50.31	0.89	4.58	5.66	0.11	15.76	21.38	0.27	0.39	0.02	99.38
BR02cpx_cp28_AVG	CORE	84.3	51.05	0.78	4.25	5.34	0.12	16.04	21.37	0.25	0.39	0.02	99.61
BR02cpx_cp29_AVG	CORE	86.0	51.20	0.74	3.77	4.81	0.11	16.57	21.44	0.25	0.66	0.03	99.56
BR02cpx_cp30_AVG	CORE	83.9	50.71	0.80	4.27	5.53	0.12	16.14	21.53	0.26	0.14	0.02	99.50
BR02cpx_cp31_AVG	CORE	85.5	51.54	0.62	3.56	5.05	0.11	16.70	21.11	0.25	0.52	0.02	99.49
BR02cpx_cp12_GM_AVG	GM	76.8	50.39	1.40	3.04	7.98	0.18	14.84	20.89	0.39	0.35	0.03	99.50
BR02cpx_cp2_RIM_AVG	RIM	78.2	50.93	1.29	2.90	7.49	0.15	15.09	20.97	0.31	0.25	0.04	99.41
BR02cpx_cp3_RIM_AVG	RIM	84.1	51.09	0.86	4.23	5.29	0.09	15.74	21.71	0.23	0.70	0.01	99.93
BR02cpx_cp7_RIM_AVG	RIM	77.2	50.45	1.52	2.92	7.88	0.16	14.94	20.79	0.35	0.20	0.03	99.24
BR02cpx_cp9_RIM_AVG	RIM	77.4	50.04	1.80	3.09	7.75	0.15	14.93	20.78	0.38	0.22	0.01	99.15
BR02cpx_cp18_RIM_AVG	RIM	77.4	50.25	1.73	3.02	7.82	0.17	15.00	20.82	0.35	0.28	0.02	99.45
BR02cpx_cp19_RIM_AVG	RIM	74.6	47.44	1.62	6.58	8.56	0.16	14.09	20.21	0.31	0.13	0.02	99.11
BR02cpx_cp25_RIM_AVG	RIM	77.3	50.50	1.54	3.08	7.87	0.16	15.06	20.84	0.35	0.27	0.02	99.67

[1]Clinopyroxene core compositions are averages of three microprobe analysis spots, whereas clinopyroxene rim compositions are averages of 1–3 analysis spots.
[2]CORE = macrocryst core analysis, GM = groundmass crystal core analysis, RIM = macrocryst rim analysis
Compositions are in weight percentages.

Appendix II. Compositions of clinopyroxene of Hvammsmúli ankaramite (data related to Paper II)

Hvammsmúli

Analysis[1]	Anal. Loc[2]	$Mg\#^{cpx}$	SiO_2	TiO_2	Al_2O_3	FeO	MnO	MgO	CaO	Na2O	Cr_2O_3	NiO	Total
Hva01_cp1_AVG	CORE	86.03	51.69	0.64	3.63	4.90	0.10	16.92	20.94	0.26	0.57	0.04	99.69
Hva01_cp2_AVG	CORE	81.78	51.09	0.95	3.72	6.24	0.12	15.72	21.48	0.27	0.19	0.02	99.79
Hva01_cp3_AVG	CORE	85.71	51.56	0.68	3.98	4.90	0.12	16.48	21.00	0.30	0.80	0.04	99.85
Hva01_cp4_AVG	CORE	85.41	51.83	0.74	3.89	5.07	0.10	16.64	21.48	0.25	0.24	0.02	100.25
Hva01_cp5_AVG	CORE	83.26	51.02	0.82	4.04	5.79	0.13	16.17	21.39	0.25	0.25	0.01	99.86
Hva01_cp6_AVG	CORE	83.54	51.29	0.79	4.02	5.68	0.12	16.18	21.50	0.25	0.21	0.02	100.05
Hva01_cp7_AVG	CORE	84.30	50.81	0.85	4.34	5.31	0.10	15.99	21.58	0.26	0.26	0.03	99.52
Hva01_cp8_AVG	CORE	78.47	50.47	1.18	3.45	7.47	0.17	15.27	20.94	0.29	0.16	0.02	99.42
Hva01_cp9_AVG	CORE	81.88	51.09	0.91	3.57	6.28	0.14	15.91	21.52	0.24	0.14	0.01	99.81
Hva01_cp10_AVG	CORE	79.20	50.62	1.20	3.44	7.21	0.14	15.39	21.16	0.27	0.15	0.00	99.59
Hva01_cp11_AVG	CORE	86.09	51.86	0.64	3.64	4.83	0.10	16.76	21.45	0.24	0.44	0.03	99.99
Hva01_cp12_AVG	CORE	86.01	52.24	0.55	3.03	5.00	0.11	17.26	21.00	0.24	0.48	0.03	99.95
Hva01_cp13_AVG	CORE	86.32	51.86	0.58	3.23	4.79	0.11	16.94	21.13	0.26	0.63	0.02	99.55
Hva01_cp14_AVG	CORE	87.21	52.06	0.55	2.96	4.48	0.11	17.14	21.01	0.26	0.88	0.03	99.48
Hva01_cp15_AVG	CORE	84.21	51.07	0.78	4.12	5.46	0.11	16.33	21.27	0.24	0.39	0.02	99.78
Hva01_cp16_AVG	CORE	84.50	51.57	0.70	3.71	5.42	0.12	16.58	21.21	0.24	0.26	0.02	99.82
Hva01_cp17_AVG	CORE	82.47	51.01	0.94	3.89	6.08	0.12	16.03	21.59	0.27	0.21	0.01	100.15
Hva01_cp18_AVG	CORE	86.10	51.57	0.64	3.52	4.80	0.11	16.67	21.34	0.26	0.69	0.02	99.60
Hva01_cp19_AVG	CORE	83.07	50.99	0.87	3.97	5.86	0.11	16.14	21.31	0.24	0.20	0.03	99.73
Hva01_cp20_AVG	CORE	84.88	51.33	0.68	3.82	5.23	0.11	16.49	21.11	0.26	0.54	0.02	99.61
Hva01_cp1_RIM_AVG	RIM	70.55	49.89	1.80	2.88	10.34	0.21	13.90	20.35	0.37	0.01	0.01	99.76
Hva01_cp2_RIM_AVG	RIM	72.68	50.55	1.72	2.86	9.51	0.21	14.19	20.61	0.34	0.12	0.02	100.10
Hva01_cp3_RIM_AVG	RIM	73.59	50.52	1.60	2.96	9.18	0.20	14.35	20.63	0.35	0.14	0.01	99.93
Hva01_cp5_RIM_AVG	RIM	73.85	50.68	1.49	2.69	9.21	0.20	14.59	20.53	0.36	0.13	0.01	99.86
Hva01_cp9_RIM_AVG	RIM	73.35	50.53	1.54	2.63	9.38	0.19	14.48	20.50	0.35	0.07	0.02	99.67
Hva01_cp11_RIM_AVG	RIM	72.51	51.14	1.47	2.25	9.79	0.21	14.49	20.41	0.35	0.00	0.02	100.14
Hva01_cp13_RIM_AVG	RIM	70.64	49.80	1.82	2.94	10.30	0.21	13.90	20.22	0.36	0.02	0.02	99.59
Hva01_cp15_RIM_AVG	RIM	72.16	50.96	1.37	2.08	10.04	0.23	14.60	20.16	0.33	0.03	0.01	99.79
Hva01_cp16_RIM_AVG	RIM	72.45	50.77	1.48	2.29	9.83	0.21	14.50	20.44	0.33	0.02	0.02	99.91
Hva01_cp5_RIM_AVG	RIM	72.97	50.42	1.37	2.81	9.57	0.19	14.50	20.41	0.35	0.07	0.01	99.69
Hva01_cp10_RIM_AVG	RIM	73.48	50.25	1.61	2.94	9.20	0.19	14.29	20.73	0.34	0.18	0.02	99.74
Hva01_cp9_RIM_AVG	RIM	74.19	50.69	1.53	2.84	9.03	0.18	14.56	20.70	0.33	0.17	0.01	100.02

[1]Clinopyroxene core compositions are averages of 3 microprobe analysis spots, whereas clinopyroxene rim analyses are averages of 1–3 analysis spots.

[2]CORE = macrocryst core analysis, RIM = macrocryst rim analysis

Compositions are in weight percentages.

Appendix III. Electron microprobe analyses of spinel of Brattaskjól ankaramite (data related to Paper II)

Analysis	SiO_2	TiO_2	Al_2O_3	FeO	MnO	MgO	V_2O_3	Cr_2O_3	NiO	Total
BR02_Ol92_sp1_1	0.10	1.52	14.70	20.49	0.18	13.87	0.11	46.93	0.17	98.06
BR02_Ol92_sp1_2	0.12	1.56	15.21	20.21	0.21	14.05	0.18	47.07	0.20	98.79
BR02_Ol93_sp1_1	0.12	1.53	13.32	20.19	0.20	13.58	0.15	48.39	0.23	97.71
BR02_Ol94_sp1_1	0.08	1.55	13.88	22.20	0.20	12.92	0.18	45.97	0.19	97.17
BR02_Ol41_sp1_1	0.08	1.57	12.11	20.81	0.19	13.25	0.14	50.94	0.16	99.25
BR02_Ol41_sp1_2	0.08	1.56	12.06	21.63	0.19	12.56	0.15	51.18	0.19	99.60
BR02_Ol41_sp2_1	0.09	1.50	12.13	24.22	0.24	10.93	0.14	50.09	0.14	99.47
BR02_Ol41_sp3_1	0.07	1.58	12.13	20.05	0.20	13.59	0.14	51.60	0.20	99.56
BR02_Ol35_sp1_1	0.10	1.49	14.51	23.49	0.21	11.84	0.15	47.70	0.18	99.67
BR02_Ol35_sp1_2	0.10	1.53	14.67	23.37	0.24	11.74	0.14	47.96	0.16	99.91
BR02_Ol03_sp1_1	0.09	1.43	10.80	23.28	0.27	11.64	0.17	50.17	0.14	97.99
BR02_Ol03_sp2_1	0.10	1.41	13.46	21.89	0.22	12.84	0.14	48.82	0.16	99.03
BR02_Ol03_sp3_1	0.08	1.52	13.42	22.98	0.21	11.96	0.15	48.12	0.16	98.61
BR02_Ol03_sp4_1	0.10	1.45	12.45	21.81	0.23	12.51	0.16	48.87	0.18	97.76
BR02_Ol03_sp5_1	0.07	1.46	13.56	22.25	0.21	12.52	0.15	48.40	0.14	98.75
BR02_Ol03_sp6_1	0.11	1.54	13.40	21.94	0.23	12.94	0.16	48.84	0.17	99.33
BR02_Ol04_sp1_1	0.11	1.61	13.31	21.94	0.22	12.86	0.15	48.24	0.14	98.57
BR02_Ol72_sp1_1	0.07	1.25	11.50	25.65	0.24	9.82	0.13	49.97	0.09	98.73
BR02_Ol95_sp1_1	0.10	1.40	11.92	27.76	0.30	8.86	0.14	47.04	0.10	97.61
BR02ts_Ol01_sp1_1	0.11	1.60	15.03	20.04	0.19	14.13	0.15	47.30	0.20	98.75
BR02ts_Ol01_sp1_2	0.12	1.68	15.01	19.79	0.18	13.92	0.15	47.29	0.20	98.34
BR02ts_Ol02_sp2_1	0.46	1.47	11.87	21.17	0.23	13.71	0.14	49.25	0.17	98.47
BR02ts_Ol04_sp1_1	0.07	1.39	11.91	21.15	0.23	12.34	0.15	51.35	0.17	98.74
BR02ts_Ol04_sp1_2	0.07	1.39	11.88	20.48	0.24	12.70	0.13	52.27	0.15	99.31
BR02ts_Ol04_sp1_3	0.09	1.38	11.88	20.83	0.20	12.55	0.14	50.48	0.16	97.70

Compositions are in weight percentages.

Appendix IV. Electron microprobe analyses of spinel of Hvammsmúli ankaramite (data related to Paper II)

Analysis	SiO_2	TiO_2	Al_2O_3	FeO	MnO	MgO	V_2O_3	Cr_2O_3	NiO	Total
Pos-1a_Ol01_sp1_1	0.07	1.57	13.38	25.63	0.24	9.94	0.17	48.20	0.19	99.39
Pos-1a_Ol01_sp2_1	0.08	1.62	13.54	24.72	0.26	10.25	0.14	48.21	0.17	98.97
Pos-1a_Ol01_sp2_2	0.08	1.64	13.53	25.00	0.23	10.31	0.18	48.64	0.18	99.79
Pos-1a_Ol06_sp1_1	0.04	2.64	14.64	20.83	0.23	12.45	0.22	48.69	0.22	99.96
Pos-1a_Ol45_sp1_1	0.06	2.04	17.43	21.64	0.22	12.76	0.18	44.79	0.16	99.28
Pos-1a_Ol45_sp3_1	0.11	1.47	17.39	22.30	0.20	12.03	0.15	45.41	0.16	99.22
Pos-1a_Ol45_sp2_2	0.08	1.51	18.12	21.54	0.22	12.85	0.16	45.10	0.18	99.75
Pos-1a_Ol45_sp4_1	0.09	1.73	16.00	22.52	0.23	11.96	0.20	47.08	0.18	99.97
Pos-1a_Ol19_sp1_1	0.07	1.44	18.42	19.07	0.20	13.79	0.14	46.19	0.21	99.54
Pos-1a_Ol19_sp2_1	0.09	1.61	20.69	18.89	0.19	14.32	0.15	44.25	0.22	100.41
Pos-1a_Ol20_sp1_1	0.07	1.35	21.78	22.57	0.24	12.63	0.18	39.83	0.16	98.81
Pos-1a_Ol20_sp2_1	0.06	1.38	21.48	22.81	0.21	12.55	0.21	39.58	0.16	98.44
Pos-1a_Ol20_sp3_1	0.05	1.50	21.13	24.12	0.19	11.89	0.23	40.61	0.16	99.87
Pos-1a_Ol20_sp5_1	0.06	1.58	21.92	24.33	0.24	12.02	0.20	39.97	0.17	100.49
Pos-1a_Ol20_sp4_1	0.05	1.46	22.30	23.52	0.20	12.39	0.23	39.74	0.15	100.03
Pos-1a_Ol22_sp1_1	0.09	1.40	15.86	20.33	0.21	12.83	0.17	47.87	0.19	98.95
Pos-1a_Ol46_sp1_1	0.06	1.50	16.71	22.62	0.24	11.98	0.21	46.28	0.16	99.76
Pos-1a_Ol26_sp1_1	0.08	1.56	16.09	21.64	0.23	12.48	0.20	47.66	0.12	100.05
Pos-1a_Ol47_sp1_1	0.07	1.42	12.70	21.20	0.21	11.50	0.18	51.69	0.15	99.11
Pos-1a_Ol48_sp1_1	0.06	1.64	19.37	25.92	0.24	11.08	0.22	40.86	0.17	99.55
Pos-1a_Ol49_sp1_1	0.05	1.11	9.03	28.54	0.31	7.78	0.18	52.24	0.13	99.38
Pos-1a_Ol49_sp2_1	0.05	1.18	9.31	28.65	0.27	7.55	0.17	50.67	0.14	97.99
Pos-1a_Ol50_sp1_1	0.08	1.47	11.67	27.15	0.27	8.90	0.23	49.13	0.13	99.02

Compositions are in weight percentages.

Basaltic magmas originate from melting of the Earth's mantle, evolve in transit through the Earth's crust and sometimes surface as orange-glowing lavas. Consequently, these lavas carry the imprint of their mantle source and the subsurface anatomy of their host volcanoes. In this thesis, I follow the evolutionary history of basaltic lavas in Iceland from mantle melting to lava emplacement by utilizing microanalyses of mineral phases, analyses of whole-rock samples and numerical modelling. I give special attention to compositions of primitive olivine macrocrysts, used as indicators of mantle melting conditions, and the Eyjafjallajökull volcanic system, for which I studied crystallization conditions of mineral phases in two primitive lavas. These investigations exposed a signature of deep melting of Earth's mantle below South Iceland and mid-crustal storage and crystallization conditions for the studied Eyjafjallajökull lavas.

Department of Geosciences and Geography A81
ISSN-L 1798-7911
ISSN 1798-7911 (print)
ISBN 978-951-51-4930-5 (paperback)
ISBN 978-951-51-4931-2 (PDF)
http://ethesis.helsinki.fi/

Painosalama
Turku 2020

UNIVERSITY OF HELSINKI
FACULTY OF SCIENCE

UNIVERSITY OF ICELAND